

FULL-SCALE STUDY OF INFRARED THERMOGRAPHY FOR ASSESSING
SURFACE AND SUBSURFACE DEFECTS IN PAVEMENTS AND OTHER CIVIL
INFRASTRUCTURE

by

Aidin J. Golrokh



A thesis

submitted in partial fulfillment

of the requirements for the degree of

Master of Science in Civil Engineering

Boise State University

August 2019

© 2019

Aidin J. Golrokh

ALL RIGHTS RESERVED

BOISE STATE UNIVERSITY GRADUATE COLLEGE

DEFENSE COMMITTEE AND FINAL READING APPROVALS

of the thesis submitted by

Aidin J. Golrokh

Thesis Title: Full-Scale Study of Infrared Thermography for Assessing Surface and Subsurface Defects in Pavements and Other Civil Infrastructure

Date of Final Oral Examination: 09 May 2019

The following individuals read and discussed the thesis submitted by student Aidin J. Golrokh, and they evaluated his presentation and response to questions during the final oral examination. They found that the student passed the final oral examination.

Yang Lu, Ph.D. Chair, Supervisory Committee

Dylan Mikesell, Ph.D. Member, Supervisory Committee

Mojtaba Sadegh, Ph.D. Member, Supervisory Committee

The final reading approval of the thesis was granted by Yang Lu, Ph.D., Chair of the Supervisory Committee. The thesis was approved by the Graduate College.

DEDICATION

This is the least that I can dedicate to my best fans in life, my mother and my father.

ACKNOWLEDGEMENTS

I need to thank my advisor, Dr. Yang Lu, for his useful ideas, important feedback and most of all, for him being there for me and offering his unconditional help and support. He is the reason why I had this wonderful opportunity and for that, I am always grateful. I also need to thank Dr. Dylan Mikesell from the department of Geosciences who kindly accepted my invitation to be my committee member and who gave me very important feedback, which made my research more useful. I am also grateful to Dr. Mojtaba Sadegh who helped me with his useful and detailed insights throughout the process of writing and defending my thesis.

My special gratitude goes to Aminul Islam, who has been a knowledgeable colleague and companion throughout these years. I should also thank my colleagues and friends from the department of Civil Engineering, including Austin Berry, Asif Rahman, Kody Johnson, Fazle Rabbi, Thomas Robbins, Taeyun Kong, Jenn Mcatee, Mariah Fowler, MD Jibon, Rhonda Magill and many more.

ABSTRACT

Infrared thermography (IRT) is an effective non-destructive testing method in the field of concrete and asphalt pavement inspection. IRT is used to have an initial evaluation of the surface and near surface of pavements in a very time effective manner compared to other types of nondestructive testing (NDT) methods. Different aspects of IRT and its use to assess surface and subsurface defects in different types of pavements are being studied and evaluated in our research group. The effect of the depth of delamination inside concrete pavement on an IRT technique is being studied. It is suggested by our group that there is a correlation between the surface crack profile on asphalt pavements and its temperature, which will help us to evaluate pavement performance condition. Finally, a full laboratory study is being conducted to experimentally quantify the effects of weather conditions and surface coating on the ability of IRT to assess surface cracks on both asphalt and concrete pavements.

TABLE OF CONTENTS

DEDICATION	iv
ACKNOWLEDGEMENTS	v
ABSTRACT	vi
LIST OF TABLES	x
LIST OF FIGURES	xi
LIST OF ABBREVIATIONS	xiv
CHAPTER ONE: INTRODUCTION.....	1
References	5
CHAPTER TWO: CONCRETE PAVEMENT SERVICE CONDITION ASSESSMENT USING INFRARED THERMOGRAPHY	6
Abstract	6
Introduction.....	7
Benefits and limitations of IRT.....	9
Test Setup.....	10
Experimental results.....	13
Interpretation of Temperature Versus Distances’ Graph	15
Image Processing Data.....	17
Modeling the IR Test	21
Integration of Simulation and Experimental Result.....	23
Conclusion	25

References.....	26
CHAPTER THREE: A REAL-TIME THERMAL IMAGING-BASED SYSTEM FOR ASPHALT PAVEMENT SURFACE DISTRESSES INSPECTION AND 3D CRACK PROFILING.....	29
Abstract.....	29
Introduction.....	30
Pavement Surface Thermal Field.....	32
IRT Mechanisms.....	34
IRT Time Window.....	35
Statistical Approaches.....	36
Analysis of Variance Test.....	36
Regression Test.....	39
Experimental Methodology.....	39
Crack Profile Data Collection.....	39
IR Thermal Image Collection.....	40
Test Setup and Data Collection for Passive IRT.....	44
Results and Analysis.....	47
Conclusion.....	55
References.....	56
CHAPTER FOUR: A FULL-SCALE EXPERIMENTAL STUDY OF THE EFFECTS OF DIFFERENT CLIMATE CONDITIONS ON INFRARED THERMOGRAPHY AND SURFACE DELAMINATION ASSESSMENT IN CONCRETE STRUCTURES	59
Abstract.....	59
Introduction.....	61
IRT Concepts and Physics.....	62

Environmental Factors	65
Methodology	68
Result	74
Comparison of the temperature decay at the crack bottom surface versus crack top edge for controlled heating, heating with airflow (wind) and humid heating (Cases #1 through #9).....	75
Comparison of the Effect of Different Humidity Levels on Temperature Decay of the Crack in Humid Heating (Cases #10, #11, #12, #13 And #14)	78
The comparison of the effect of different weather conditions and various crack depths on temperature decay of the crack and the temperature readings of thermal camera (Cases #1 through #9).....	81
Comparison of the effect of different air velocities on temperature decay of the crack (Cases #15, #16 and #17)	84
Conclusion	85
References.....	86
CHAPTER FIVE: CONCLUSION.....	89

LIST OF TABLES

Table 2- 1.	Area comparison	21
Table 3- 1.	ANOVA table of equations.....	38
Table 3- 2.	Preliminary results based on three groups of temperature data points	48
Table 3- 3.	Total number of measurements, total number of groups and correction factor	49
Table 3- 4.	ANOVA table	49
Table 4- 1.	Experimental tests performed inside the laboratory	73

LIST OF FIGURES

Figure 2- 1.	(A). Visual image of the specimen, (B). Thermal image of specimen with defects that are inserted in the depth of 2 centimeters (Heated up using heat blower)	14
Figure 2- 2.	(A). Specimen with defects that are inserted in the depths of 5 and 10 millimeters (Heated up using an oven), (B). Specimen with defects that are inserted in the depth of 5 and 10 millimeters (Heated up using heat blower) – Image is taken 2 minutes into the cooling cycle, (C). Specimen with defects that are inserted in the depth of 5 and 10 millimeters (Heated up using heat blower) – Image is taken 20 minutes into the cooling cycle	14
Figure 2- 3.	Line 1 is used to plot a temperature related graph of the surface of the specimen	16
Figure 2- 4.	Temperature versus distance graph assigned to line 1 in Figure 3	17
Figure 2- 5.	Thermal image after application of color filter	18
Figure 2- 6.	(A). Processed image using a 37 degrees of Celsius threshold, (B). A comparison between the actual size of the delamination and its size in the processed image	19
Figure 2- 7.	Defects location in the software model.....	22
Figure 2- 8.	Line that is used to plot a temperature related graph of the surface of specimen	22
Figure 2- 9.	Temperature-length graph assigned to the line in Figure 2-8	23
Figure 2- 10.	Comparison between the location of defects on both camera and software graphs	24
Figure 3- 1.	Surface delamination temperature gradient	32
Figure 3- 2.	Correlation between depth and width and temperature	40
Figure 3- 3.	Mobile thermography testing setup	41

Figure 3- 4.	Visual versus thermal images	42
Figure 3- 5.	Processed image.....	44
Figure 3- 6.	Measuring depth and width of crack using digital caliper	46
Figure 3- 7.	Thermocouple is used for measuring the mean temperatures inside cracks	46
Figure 3- 8.	Boxplot of temperature data points which are separated into three groups with similar ambient air temperatures and weather conditions	48
Figure 3- 9.	Relationship between depth and the highest temperature that is recorded from the crack	50
Figure 3- 10.	Calculation of the average ambient surface temperature	51
Figure 3- 11.	Relationship between width and point-wise normalized temperature based on average ambient surface temperature.....	53
Figure 3- 12.	Relationship between depth and normalized temperature based on average ambient surface temperature	54
Figure 4- 1.	Surface crack temperature gradient	62
Figure 4- 2.	The temperature reading process of thermal camera in experimental tests	65
Figure 4- 3.	The effect of wind on convective heat transfer on the surface of the concrete A) Under direct sun exposure B) Under indirect sun exposure (Shadow)	67
Figure 4- 4.	Width, depth, and highest temperature measurements in surface cracks .	69
Figure 4- 5.	Laboratory crack sample: A: Crack width, B: Crack depth.....	70
Figure 4- 6.	Controlled laboratory testing system	71
Figure 4- 7.	Distance between the test facilities and crack: A: Distance between Thermal camera and crack= 70 cm, B: Distance between halogen lamp and crack= 10 cm, C: Distance between fan and crack= 30. 5 cm, D: Distance between humidifier and crack= 55 cm.....	73
Figure 4- 8.	(A & B) Foggy weather test setup (Humidity=~100%).....	74

Figure 4- 9.	Temperature gradient captured by the infrared thermal camera during the heating and cooling cycles (Crack sizes: Width=1cm Depth=3.7cm) - Highest surface temperature is calculated in each image	75
Figure 4- 10.	Temperature decay versus time for top edge and bottom of crack in 3 different test sets, A) Controlled heating, B) heating with airflow and C) moist heating.....	77
Figure 4- 11.	Relation between humidity and ambient air temperature decay:	78
Figure 4- 12.	The change in humidity levels versus time.....	79
Figure 4- 13.	Time versus temperature decay graph for different humidity levels	80
Figure 4- 14.	The effect of different weather conditions on temperature reading of the thermal camera for a crack with 1 cm width and 5.2 cm depth	81
Figure 4- 15.	Comparison of the effect of different weather conditions on temperature reading of the thermal camera for cracks with varying crack profiles: A: For width=1 cm and depth=3.7 cm, B: For width=0.5 cm and depth=1 cm	83
Figure 4- 16.	Comparison of the percentage of difference for varying depths when exposed to different weather conditions	83
Figure 4- 17.	Temperature decay in different wind (air) speeds	84

LIST OF ABBREVIATIONS

ASCE	American Society of Civil Engineers
NDT	Nondestructive Testing
ASTM	American Society for Testing and Materials
POA	Percentage of Accuracy
HMA	Hot Mixed Asphalt
ANOVA	Analysis of Variance
DOF	Degree of Freedom
IRT	Infrared Thermography
GPR	Ground Penetration Radar
UT	Ultrasonic Test
POD	Percentage of Difference

CHAPTER ONE: INTRODUCTION

It is safe to claim that the field of monitoring is going to be essential in the upcoming decades in both the United States and other parts of the world. In a report from the American Society of Civil Engineers (ASCE), the condition of America's infrastructure is depicted and assigned a low grade which indicates a deteriorating infrastructure which needs improvements to ensure a more thriving future. According to an ASCE report, the cost of remediation and retrofitting of infrastructure in the United States is \$1.3 trillion (Hu et al. 2002). In a more specific field of civil engineering, it is claimed that each year more than \$2 billion is spent by infrastructure management agencies in the United States to maintain concrete bridge decks (Kee et al. 2012).

In order to maximize the working efficiency with limited sources to address such huge numbers related to assessment of infrastructure, prioritizing our maintenance actions based on the expected current condition of structures becomes even more essential. The methods that are used to monitor the structure condition fall under two main categories that are destructive and nondestructive tests. As the name suggests, in destructive testing at least a section of the structure needs to be destroyed to be able to investigate the presence of the anomaly. This obviously is not an option when it comes to many types of civil infrastructures. Nondestructive tests however are a reliable substitute in many cases of monitoring the infrastructure because they enable us to gather data on the field without damaging or destroying the structure. There are many different nondestructive testing methods available out there such as IRT, ultrasonic, ground

penetration radar and so on. Between these NDTs, IRT is normally chosen as a substitute for a fast and easy monitoring and inspection technique.

This is where methods such as infrared thermography (IRT) can help to assess the aging infrastructures so that we can spend money efficiently. IRT is the use of temperature data acquired from thermal imagery to study heat distribution in structures or regions. It is the process of using a thermal imager to detect infrared radiation (heat) that is emitted by an object. IRT is effective, repeatable, convenient to the public, economical and the fastest and easiest nondestructive testing (NDT) method in terms of data collection.

Thermography is used effectively in many different fields. In medicine, the ability of infrared camera to detect heat patterns and blood flow in body tissues is helpful for cancer diagnoses. The idea behind this test is that, as cancer cells multiply, they need more oxygen-rich blood to grow. When blood flow to the tumor increases, the temperature around it rises. In electronics, a key factor in the design, tests, verification and troubleshooting of all electronics, is heat management, since all electronics operate with current flowing, which in turn leads to power dissipation. This power dissipation manifests itself primarily in the form of heat. In mechanical engineering, the technology helps to validate normal operations and, more importantly, locate thermal anomalies (abnormal patterns of heat invisible to the eye) which indicate possible faults, defects or inefficiencies within a system or machine asset.

In civil engineering, the fact that there will always be a temperature gradient between anomaly and intact area of civil structures, when they are exposed to heat, is the basis for the use of thermography in the field of defect assessment. There are many

different applications in which IRT can be used to determine the conditions and assess the characteristics of structures and infrastructures. One application is the thermal mapping of surface defects on an asphalt pavement road by using an assembled infrared camera on a car (ASTM, 2014 speed limit for IRT: 16 km/h (10 mph)). Assessing surface defects on bridge barriers and soffits is the basis of another application. The same notion can be used to assess subsurface defect detection on bridge decks using temperature gradients acquired from thermography. IRT can also help us study asphalt mixture segregation on a freshly paved HMA and other information that is used to quantify the asphalt pavement homogeneity and to develop the quality assurance criteria to be used in paving contracts.

Different aspects of IRT and its use to assess surface and subsurface defects in different types of pavements are being studied and evaluated in our research. The model of the camera that is used in all experiments is a FLIR T430sc 2.0 infrared thermal camera with a resolution of 320 by 240 pixels.

In our first publication, the effect of the depth of delamination inside concrete pavement on infrared thermography technique is studied. The method of thermography was active in which a heat source was used to heat up the surface and extract a temperature gradient from the surface of the specimen.

It is suggested in our second publication that there is a correlation between the surface crack profile on asphalt pavements and its temperature, which will help us to evaluate pavement performance conditions. This was a field test that was conducted on the surface of the asphalt pavement. Given the fact that cracking may impair the durability of concrete by allowing immigration of external aggressive agents, crack

monitoring is always a vital part in building and pavement pathology. In this test we used thermography to assess cracks on top of asphalt pavements by using the information that we attain from thermography. It should be noted that the use of thermography to assess surface cracks is more scarce compared to subsurface defect assessment and the study of correlation for pavements is something that has not been done before.

Finally, in our most recent publication, a full laboratory study is conducted to experimentally quantify the effects of weather conditions and surface coating on the ability of IRT to assess surface cracks on both asphalt and concrete pavements. This is an important study since surrounding environmental conditions have major effects on surface and crack temperature. IRT technology can be affected by critical environmental conditions such as sunlight, ambient temperature variation, wind speed and humidity. Many researches have mentioned the importance of the effect of weather conditions but no research is dedicated to experimentally quantifying the effect. Around 90 different tests have been conducted from which 1050 unique data points have been extracted. Eventually, around 1,260,000 temperature data points have been gathered which gives a huge data set and will give us the opportunity to do several statistical analyses. We will also be able to compare our results with the results from computer simulation. The test setup can also be used for more weather condition related studies in the future.

In the following, each of our submitted and published papers are included in which different aspects of IRT are discussed. This can help to better understand the advantages and disadvantages of the use of IRT to monitor and assess the condition of civil infrastructures.

References

- ASTM, "Standard Test Method for Detecting Delamination in Bridge Decks Using Infrared Thermography," in Proceedings of the ASTM Designation D4788-03 ed. ASTM International, West Conshohocken, Penn, USA, 2014.
- Hu C. W., Shih J. K. C., Delpak R., Tann D. B., Detection of Air Blisters and Crack Propagation in FRP Strengthened Concrete Elements Using Infrared Thermography (2002)
- Kee S-H., Oh T., P S. J., Arndt R. W., Zhu J., Nondestructive Bridge Deck Testing with Air-Coupled Impact-Echo and Infrared Thermography (2012)

CHAPTER TWO: CONCRETE PAVEMENT SERVICE CONDITION ASSESSMENT
USING INFRARED THERMOGRAPHY

Published in Hindawi Journal (Open access)

Yang Lu^I, Aidin J. Golrokh^{II}, and MD Aminul Islam^{III}

I: Associate professor at Boise State University

II & III: Graduate research assistant at Boise State University

Abstract

Infrared Thermography (IRT) is an effective non-destructive testing method in the field of concrete pavement inspection. IRT is used in this research in order to have an initial evaluation of the surface and near surface of concrete pavement in a time effective manner. The method can be widely used for concrete pavement particularly bridge deck inspection. In this paper, the effect of the depth of delamination inside concrete pavement on infrared thermography technique is studied. To be able to mimic the delamination in subsurfaces, two Styrofoam cubes have been inserted in different depths near the surface of the concrete cylinder. After heating up the specimen, thermal images were taken from the surface using an infrared thermal camera to evaluate the effect of subsurface defects on detection sensitivity and accuracy. We also investigated the precision to which the shape and the size of the sub-surface anomalies can be perceived using an uncooled thermal camera. To achieve this goal, we used image-processing techniques to accurately compute the size of delamination to compare it with the actual size. In addition, distance/thermal graphing is used to detect the presence of the defect underneath the

concrete surface. Furthermore, thermal transfer modelling was adopted in this paper to assist the setup of this experiment and the results are compared with laboratory findings.

KEYWORDS: IR thermography, Non-destructive testing, Pavement inspection, Image processing

Introduction

Infrared thermography (IRT) is a fast and easy to use nondestructive examination method that enables us to detect near surface delamination in a wider spectrum and with an acceptable accuracy compared to visual testing methods (Titman 2001). IR inspection does not need direct contact with the surface of the bridge. IR imaging data can be collected using a camera that is installed on top of a vehicle that can travel with a speed of 16 km/h (10 mph) (ASTM 2014). These advantages give the inspector the opportunity to manage the inspection process on the bridge without interfering with the traffic (Hiasa et al. 2016).

IRT captures the temperature gradient of concrete pavement surfaces. IR cameras are going to be able to capture clear temperature gradients on the concrete pavement surface at certain time windows during heating or cooling cycles (Watase et al. 2015). When exposed to heat, delaminated parts of concrete will interrupt the heat transfer since they have a lower thermal conductivity compared to concrete, therefore spots that are located on top of the delamination will be shown as hotter than the corresponding spots on top of sound parts (Clark et al. 2003). This is actually the case when ambient heat is applied on the top surface of the specimen or structure. The heat source can be either natural, such as the sun, or artificial, such as high-power ultrasound (Mignogna and

Green Jr 1981). We should note that in the case of internal heating or applying heat from underneath the specimen, a normal practice in laboratory experiments, the surface that is exposed to the delamination will appear cooler than the sound area in a thermal image. The reason for that is the same as is mentioned earlier.

Passive and active thermal imagery are the two types of IR inspection methods (Roche et al. 2013). In a passive approach, an inspection is conducted without using artificial heating while in an active approach, a specimen is heated up artificially and then the temperature gradient is measured during heating or cooling cycles (Richter et al. 2012). One very popular type of active thermography is Pulsed Thermography (PT). In this method, the depth of the delamination can be investigated by recording the temperature decay of the specimen. After deploying heat to the specimen, the surface temperature will be recorded using a temporal plotting that gives us the temperature with respect to relative time (seconds). There will be a rapid temperature change on the surface due to thermal propagation by diffusion and radiation and convection losses. Delamination will affect the rate of diffusion, therefore, the delaminated area appears to have a different temperature when inspected using live thermal imagery. Deeper defects will have a later observation rate compared to the shallower ones. This is because the observation time (t) and the depth (z) are correlated (Cielo et al. 1987), i.e. t is in fact the square of z and the loss of contrast (c) is proportional to the cube of the depth (Allport et al. 1988):

$$t \approx \frac{z^2}{\alpha} \text{ \& } c \approx \frac{1}{z^3} \quad (2-1)$$

where α is thermal diffusivity of material (i.e. 0.53 for concrete).

Note that as part of the limitations of this approach, the radius of the smallest defect that is detectable by thermal image should be around two times larger than the depth in which it is located underneath of the surface of the specimen (Vavilov and Taylor. 1982).

After employing a heat pulse on the specimen, the temperature decay will follow the following equation (Maldague. 2001):

$$\Delta T \approx \frac{Q}{e\sqrt{\pi t}} \quad (2-2)$$

where, ΔT is the increase of the temperature on the surface, Q is the quantity of the energy absorbed, and t is considered as time. In the denominator, e is the thermal effusivity which is calculated using the following formula: $e = \sqrt{k\rho C}$, Where k is thermal conductivity (for concrete it is $1 \text{ Wm}^{-1}\text{°C}$), ρ is mass density (for concrete it is 2400 kgm^{-3}) and finally C is specific heat (for concrete it is $800 \text{ Jkg}^{-1} \text{°C}^{-1}$).

For materials of low diffusivity, a uniform heating inside the oven should be used for their preheating process. In such experiments, after the specimen reaches a stable temperature that is higher than the ambient temperature, the specimen will be removed from the oven and during its cooling cycle, the surface temperature will be recorded using an infrared camera. Then the data can be used to verify the previous equation and eventually will help us realize the depth of the defects inside the specimen (Wu et al. 1997). In later experiments, the accuracy and the workability of the aforementioned equation for concrete structures will be examined using live thermal imagery.

Benefits and limitations of IRT

IRT is a fast and reliable technique. Deployment of the procedure is easy and no direct contact is required. Its one-side deployment makes it favorable for bridges in which

we generally have access to only one side of the structure. It is considered a safe technique since there is no harmful radiation involved. A thermal camera and corresponding software will provide us a numerical thermal modeling.

On the other hand, it is difficult to manage a uniform heating in active IRT. Thermal contrast is a decaying process and due to this transitory phase, a fast recording IR camera is required. Defects are detectable only if they are located in shallow depths, especially inside concrete pavements. Finally, this system only works when there is a thermal contrast present (Maldague 2001). In order to overcome these disadvantages, we use an image analysis approach to detect the subsurface instead of interpreting the raw IR images.

Utilizing the benefits of IR techniques, we use IR to fast-detect concrete pavement subsurface defects. A laboratory-designed experiment was carried out in this study. Thermal transfer modeling was used to assist the IR imaging test setup. In our experiment, we used active thermography but we did not employ live thermal imagery. We used a specific temperature threshold (37 degrees of Celsius) to process our images and get the digital indication of the location of the defects. In this temperature, the amount of thermal energy that is defused on the surface of the specimen is calculated and deducted from the thermal image using the image processing technique.

Test Setup

In this research, we used a FLIR thermal camera, model T430sc, to capture image data. Object distance is set at 0 to 1 meter and atmospheric temperature is set at 20 degrees Celsius (close to lab temperature). Relative humidity is considered around 50 percent and emissivity was set as default that is 0.95. The wavelength range of the

camera is between 7 to 14 Microns. Integration time in the camera for our study is 12 milliseconds.

In order to use this method on the concrete and asphalt pavements in the field, it is ideal to maintain a specific temperature and humidity throughout the entire testing procedure, otherwise the changes should be included in the specifications of the camera and they should be mentioned in the results.

This model of camera uses an uncooled micro bolometer also known as a thermal detector (Kruse 2001). Thermal sensitivity of the camera is less than 0.045 degrees at around 30 degrees of Celsius with the accuracy of ± 2 percent.

This camera also uses a technique called UltraMax, which is a type of super-resolution that is an image enhancement technology, which captures a series of thermal images and combines them into a new image. UltraMax uses the natural movement of the hand to capture an image set in which each image is slightly offset from the others. This gives us a higher number of data compared to a single image. By using this technique, we managed to increase the pixels from 76800 to 307200, which will provide a better quality of thermal image.

We developed a simple procedure to fabricate lab scale concrete specimens. In order to mimic the real pavement subsurface defects, multiple delamination was introduced in the concrete cylinder. For this test we casted multiple concrete cylinders and inserted different shapes of delamination in different depths of the specimen to realize which depth is the most ideal and gives the best contrast in thermal images. The diameter of each cylinder is 10.16 centimeters (4 inches) and the height is 20.32

centimeters (8 inches). Defects are 3 by 3 and 4 by 4 square centimeter Styrofoam rectangular cubes and their height varies depending on their depths.

Our camera did not record a visible temperature change for the defects that were buried more than 3 centimeters deep inside the concrete. On the other hand, we were able to detect defects with depths in between 1 to 2.5 centimeters. For the defects with depths less than 1 centimeter, the images were clear enough for further studying.

Active heating input was provided from one end surface of the specimen. This type of heating is common for thermal inspections of specimens and the heat source can be a laser or other types of heat induction devices (Osiander et al. 1998). In order to simulate the cooling cycle of the specimen, two different types of heating procedures were used to increase the temperature. At first, the specimen was heated up using an oven for ten minutes while keeping the bottom side of the concrete inside iced water. Although this method induced uniform heat on the surface the contrast in the thermal images was not sharp enough for us to be able to use it for further evaluation. This type of heating procedure will be useful when live temperature inspection is conducted using thermal video.

In the second approach, a hot air blower was used to heat up the surface for 15 to 20 minutes. With this method we got a clearer thermal image and the edge of the defects were more visible. The highest temperature rose up to 63.7 degrees Celsius. This method of heating loosely simulates the type of ambient heating that is exposed to the bridge deck.

Experimental results

The visible image of the specimen is shown in Figure 2-1(A). The thermal image of the same specimen is on display in figure 2-1(B). Note the temperature difference at the bottom of this image, right under the cylinder, is simply the reflection of the heat from the surface of the table. There is one 4 by 4-cm³ Styrofoam cube used as a delamination that is placed at 2 centimeters deep inside the specimen. The surface is heated up to 45 degrees Celsius. The temperature of the surface that is located on top of the delamination is visibly higher than the sound area that helps us to estimate where the defects are inserted. However, the heat is expanded in a wider area than the actual size of the delamination underneath the surface. As already mentioned, the surface on top of the delamination has a higher temperature. Since concrete has a low heat conductivity, the heat will be trapped in the body of the specimen and there will be a temperature difference between the delaminated area in the middle and the edge of the specimen, which is more exposed to the surrounding air. A similar method of inspection is used inside industrial plants (Harishkumar et al. 2014). Due to this temperature difference, heat defuses from the delaminated area towards the boundary that is colder. This is one reason why the area with a higher temperature is wider than the area of the delamination itself inside the specimen.

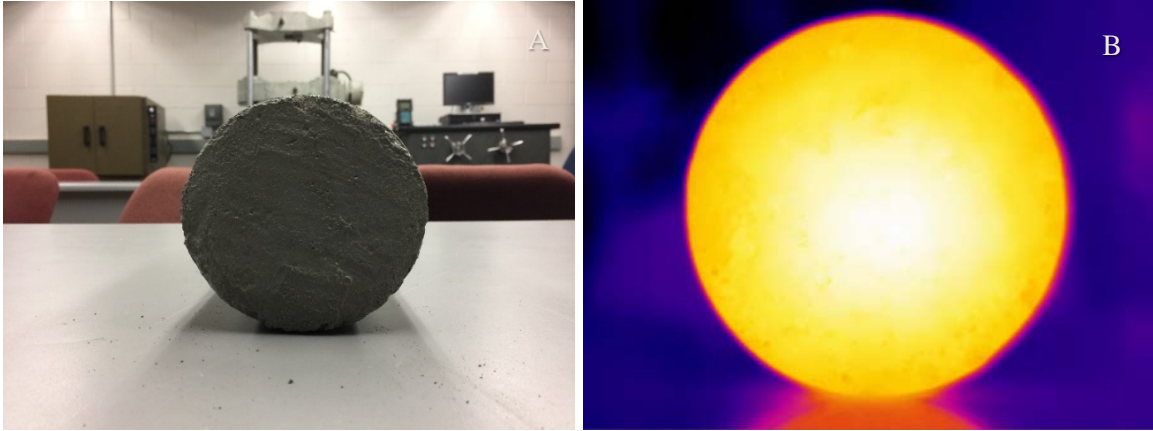


Figure 2- 1. (A). Visual image of the specimen, (B). Thermal image of specimen with defects that are inserted in the depth of 2 centimeters (Heated up using heat blower)

Using the type of the thermal camera that we have for this experiment, we can detect defects clearly under the concrete surface up to a depth of 2 centimeters.

Nevertheless, as it will be mentioned in more details in the next sections, the shallow defects, up to one centimeter, will have the clearest temperature contrast in the IR thermal images (Vollmer and Möllmann 2011).

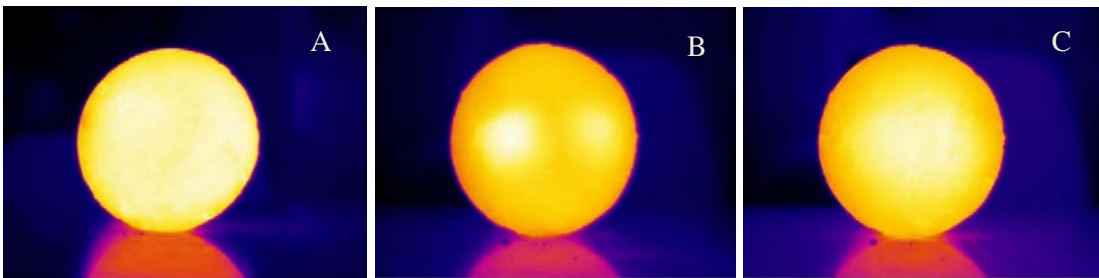


Figure 2- 2. (A). Specimen with defects that are inserted in the depths of 5 and 10 millimeters (Heated up using an oven), (B). Specimen with defects that are inserted in the depth of 5 and 10 millimeters (Heated up using heat blower) – Image is taken 2 minutes into the cooling cycle, (C). Specimen with defects that are inserted in the depth of 5 and 10 millimeters (Heated up using heat blower) – Image is taken 20 minutes into the cooling cycle

Figures 2-2(A) and 2-2(B) are of the same specimen, which has two defects (both are 3 by 3-cm³ Styrofoam cubes), inserted 5 and 10 millimeters underneath the surface.

The type of heating procedure is an important factor in terms of having a clearer thermal

image. In Figure 2-2(A), the specimen was heated up inside an oven for 30 minutes. More than 50 images were taken in a time span of 2 hours and none of them had a clear indication of defects that were trapped underneath. The heat diffusion was steady all over the surface of the specimen and there was no indication of a noticeable temperature difference to the point that it can be used for further studies.

As for Figure 2-2(B), a heat blower was used for about 20 minutes to heat up the surface. The thermal image was taken 3 minutes into the cooling cycle of the specimen. The highest temperature was around 63.5 degrees of Celsius. Temperature differences between the delaminated area and the sound area is clearly visible in this image. It also indicates that the depth has a major effect on the temperature gradient that is visible on the surface of delaminated areas of the specimen. The defect that is shallower underneath the surface has more effect on the temperature of the surface of the specimen. This difference will eventually fade away as the time passes during the cooling cycle and there will be less indication of the temperature difference between the two delaminated areas. The image in figure 2-2(C) is taken 20 minutes into the cooling cycle and the temperature difference is not clear enough therefore we cannot use a longer time span to take our images from the surface.

Interpretation of Temperature Versus Distances' Graph

A graph is plotted using the temperatures that are assigned to each pixel on line 1 (shown in Figure 2-3) that is put in the middle of the surface of the specimen. This line intersects the areas with the most temperature gradient inside the IR thermal image. By using this line, we can get the temperature of each pixel located on these areas.

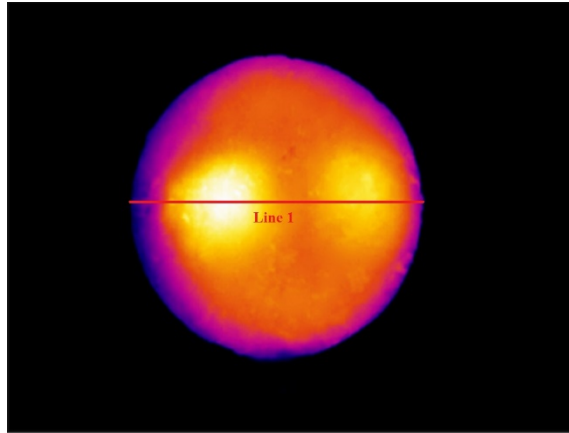


Figure 2- 3. Line 1 is used to plot a temperature related graph of the surface of the specimen

As is shown inside the graph (Figure 2-4), the location of each defect is visible with a very good accuracy. It is also clearly visible that there is a depth difference between the two defects by judging the temperature difference on Y-axis. The pattern inside this graph shows a clear connection between the depth in which the defect is located underneath the surface and the amount of temperature that is reflected from the top of the surface. In the graph, we can clearly see that there is 2 degrees Celsius temperature gap between defect 1, which has the temperature of about 61.5 degrees Celsius, and defect 2, which has the temperature of about 63.5 degrees Celsius.

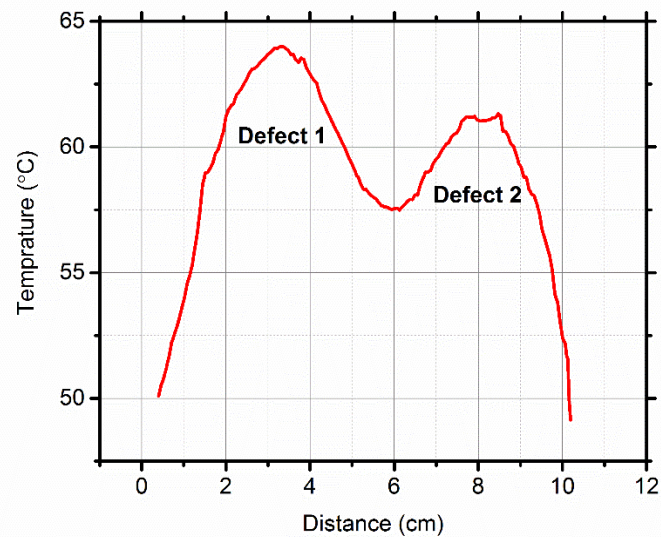


Figure 2- 4. Temperature versus distance graph assigned to line 1 in Figure 3

In live imagery, a similar graph can be used in order to get the temperature gradients during the heating or cooling cycles. The information can later be used to both locate the defects and, if possible, calculate the depth of each defect inside the concrete pavement. The relation between the depth and the observation time is already mentioned in active and passive IRT section.

Image Processing Data

As is mentioned in the previous sections, the image for the specimen with two defects inserted 5- and 10-millimeter depths underneath the surface is used for image processing purposes. For defects that are under 1 centimeter inside the concrete pavement, the thermal image presents the clearest data with best contrast that enables us to determine the edges of the delaminated area with higher temperatures. To make the image clearer we are going to use a different filter that magnifies the contrast between different sets of temperatures, to refine the difference between each temperature set. This

filter only manipulates the coloring that is assigned to each temperature pixel that results in a sharper and clearer temperature contrast inside the image (Figure 2-5).

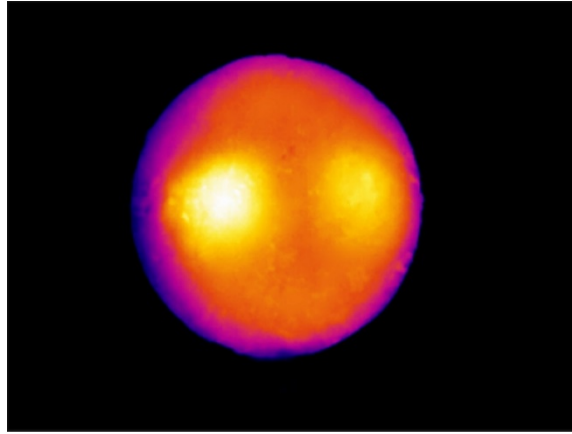


Figure 2- 5. Thermal image after application of color filter

The minimum temperature in this image is around 21 degrees Celsius and the maximum temperature is around 63.5 degrees Celsius. In the processed image, we used 255 different thresholds, known as gray thresholds, and each of these thresholds are assigned to a specific temperature. A gray threshold of 226 which corresponds to 37 degrees Celsius (Figure 2-6(A)) is used to get the best contrast between the delaminated area and the sound area. By choosing the threshold, we are eliminating all the pixels that have a temperature more than a certain degree Celsius (Ibarra-Castanedo et al. 2004). This helps us to clarify the area of the delaminated surface for further study inside the computer (Russ and Neal, 2016). In Figure 2-6(B), the actual areas of the defects are added to the processed image. This can give us a sense of the difference between the actual area and the area that the thermal camera can detect.

As is clearly shown in the processed images, for shallower delamination, the area with a higher temperature on the surface will be closer to the actual area of the surface of the delamination (Rajic, 2002). It is also worth mentioning that, in the shallower defect,

the heated area exceeds the actual area on the left side. This can be due to the heat diffusion that is caused by the temperature differences between the boundary of the cylinder and the middle part of it where the defects are located.

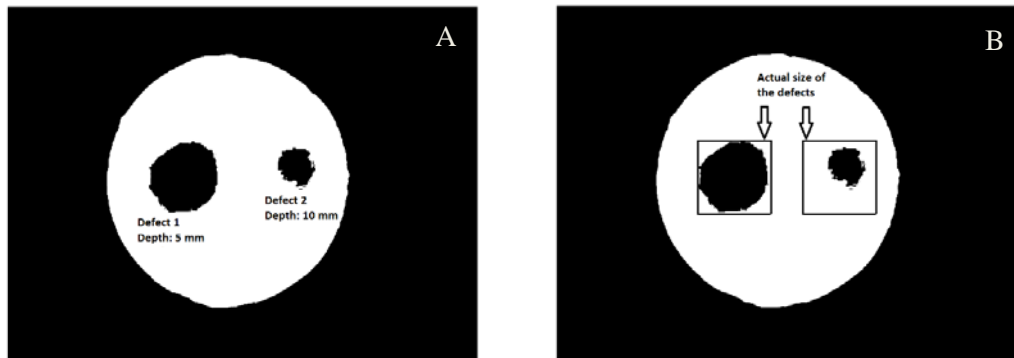


Figure 2- 6. (A). Processed image using a 37 degrees of Celsius threshold, (B). A comparison between the actual size of the delamination and its size in the processed image

The data that we got from the image processing enables us to get more information from the raw images using computer coding. Through this information, we can extrapolate mathematically accurate data to help us identify the characteristics of the delaminated areas. Table 2-1 contains an area comparison between the delaminated areas that are shown in the processed thermal image and the actual area of the surface of the defects inserted in the concrete specimen.

Using these data, we came up with a quantitative measuring method that helps us calculate the percentage of accuracy (POA) of the processed thermal image. We found the percentage of difference between the actual area of the delamination and the area that is shown in the processed image. Using POA, we can come up with a system that enables us to evaluate the area of an unknown delamination in accordance to its depth underneath the surface of the concrete specimen. We should note that the temperature threshold that

we use is the main factor in determining POA, i.e. if we choose a bigger threshold we may end up having entirely different POA. In some cases, when the threshold is bigger than a certain number, the delaminated area in the processed image will overlap the actual size of the delamination. Of course, choosing such a threshold is not going to be favorable for our purpose.

Since we know the actual diameter of the cylinder, in order to calibrate the processed image, we drew a line from either ends of the cylinder borders. This line occupies 587.82 pixels in the processed image and since we know that the diameter of the cylinder is 10.16 centimeters, the number of pixels in each centimeter can be calculated which is 58 pixels for each centimeter of the image. Therefore, there are 3364 pixels in every square centimeter of the image. Using this number, we came up with Table 2-1 for our area comparison.

Table 2- 1. Area comparison

	Number of Pixels	IR measurement of area	Percentage of Accuracy (POA)
Actual Area of the defects inside the specimen	30276	9 cm ²	100 %
Area of processed image of the 5 mm-deep defect	21286	6.33 cm ²	$\frac{6.33}{9} \times 100=70.33$ %
Area of processed image of the 10 mm-deep defect	5727	1.7 cm ²	$\frac{1.7}{9} \times 100=18.88$ %

According to the data that is extrapolated from the processed image, the delamination that is located at a depth of 5 millimeters inside the concrete pavement has a POA of more than 70 percent with respect to the actual size. The POA drastically decreases when the delamination is 5 millimeters deeper. This clearly shows that the accuracy of the thermal image is strongly related to the depth of the delamination underneath the surface.

Modeling the IR Test

Heat transfer in solids is simulated inside the computer to further understand the IR test setup (Cannas et al., 2012). Concrete is the main material and Styrofoam cubes are used as for the defects underneath the surface. A heat source of 300 watts per meter cubed is applied on top of the concrete in a uniform pattern and the bottom side was kept at 0 degrees Celsius to see the heat diffusion inside the model (Figures 2-7 and 2-8). The defects are of the same size as the defects in our experimental model and they are put in the same exact depths as well.



Figure 2- 7. Defects location in the software model

As it is shown in Figure 2-8, a guideline is put on top of the model that covers the surface on top of the defects and their surrounding sound areas. This line was used to extrapolate a temperature-distance graph from the model. This will help us to detect the defects underneath the model as we did in the actual experimental test and it helps us to learn about the depth difference between the two delaminations by using the data that is shown inside the graph.

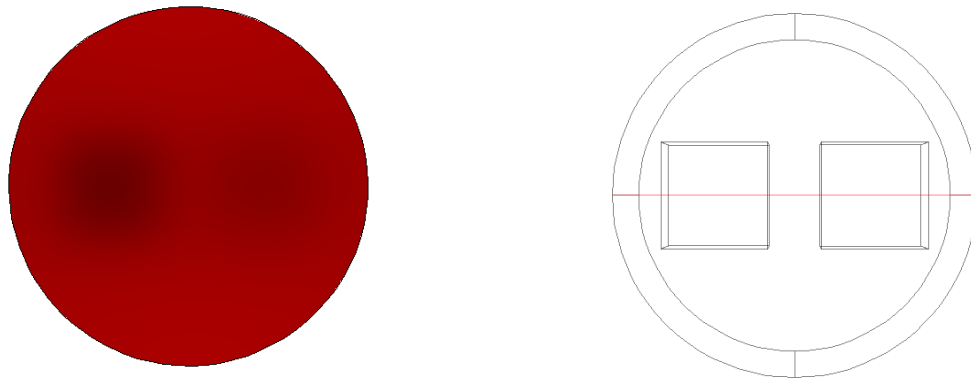


Figure 2- 8. Line that is used to plot a temperature related graph of the surface of specimen

In the software model, temperature contours show all areas with the same unique temperature compared to their surrounding area (Gerlich et al. 2013). As it will be explained in more details in the next section, since our heating process in the

experimental test was not uniform, the heated areas are different in the software results from the actual experimental results especially on the deeper defected area.

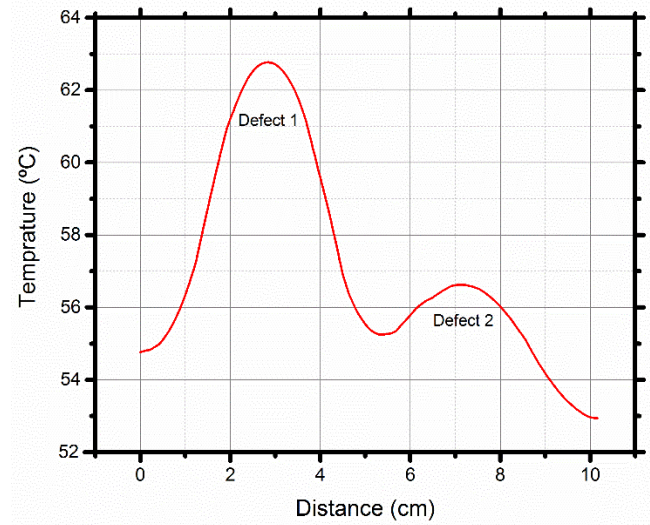


Figure 2- 9. Temperature-length graph assigned to the line in Figure 2-8

This graph from the model (Figure 2-9) follows the same pattern that we got from experimental data. From this graph, the same as the experimental graph, we can come up with a pattern that gives a relation between the temperature difference and the depth in which the defects are located.

Integration of Simulation and Experimental Result

Judging the temperature graphs extrapolated from both experimental data and the data from the software, we realize that both graphs follow the same pattern. The maximum temperature, which is located on top of the shallower delamination, is almost the same in both graphs with a magnitude close to 63.5 degrees Celsius in the experimental graph and 62.5 degrees Celsius in the simulation graph. On the other hand, there is a temperature difference between the simulation and experimental data when it comes to the temperature on top of deeper delamination. This can be because in the software we applied a totally uniform heat flux to the top surface of the cylinder but, our

heating process, which was done using a heat blower, was not performed in a uniform manner.

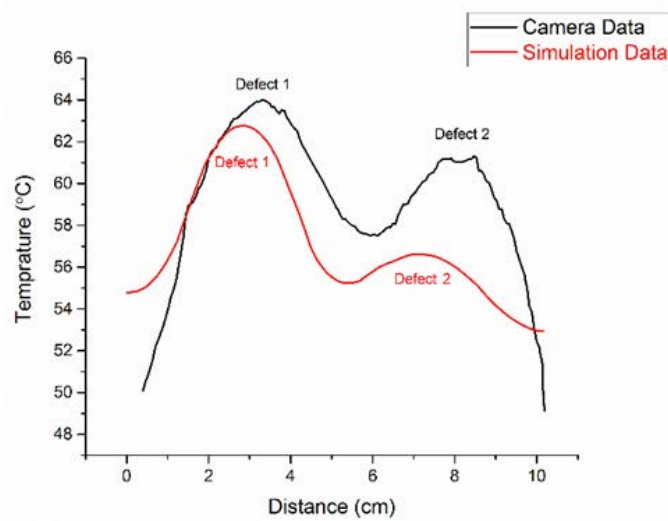


Figure 2- 10. Comparison between the location of defects on both camera and software graphs

In future experiments and to get closer results to what we get from the software we can use more uniform ways of inducing heat such as putting the specimen on a hot surface for a certain amount of time and then taking thermal images from it. In Figure 2-10, a distance versus temperature graph for both simulation and experimental data is shown for comparison. In this graph, we can clearly see that our simulation and experimental data are following the same pattern when it comes to the relationship between the depth of defects and the temperature of the surface of the specimen.

Since we were able to confirm the pattern between the depth of the delamination and the temperature on the surface of the model in both the experimental test and the software, in future studies we can use this pattern in the software and predict the results that we will get from experimental tests. This will help us to optimize our experiments inside the software before we start the process inside the lab.

Conclusion

In our research, an experimental test has been conducted on a concrete specimen with two defects located at different depths. One defect is located at 5 millimeters and the other one is located at around 10 millimeters underneath the surface of the specimen. After inducing heat on the surface of the specimen for a certain amount of time, thermal images have been taken and then used for further studies.

A temperature versus distance graph is drawn using the data that we got from thermal images. A clear pattern has been found between the temperature gradient and the depths of the defects underneath the surface. There is a 2 degrees Celsius temperature difference between the surfaces on top of the two defects. As it is shown inside the graph, deeper defects trapped less heat on top of it therefore the camera read less temperature from the top surface of the deeper defect compared to the shallower defect.

A simulated model of the same test has been conducted inside the computer and the results have been compared with the ones that were extrapolated from the experimental test. The comparison showed us a clear link between the experimental and software results. We also have witnessed the same pattern in the graph that we got from the software. In this graph, the temperature difference between the surfaces on top of each defect is around 6 degrees Celsius. That is noticeably more than the temperature difference that we got from the experimental data because in our simulation we used a uniform heating process on the surface while this was not the case in our experimental test.

The same thermal image then was used for image processing purposes and the difference between the areas of the processed image of the defects and the actual size of

the defects has been found. The area of the defect that is placed at 5-millimeters depth inside of the specimen is about 6.33 cm² which is 30 percent less than the actual size of the specimen which is 9 cm². The size of the defect that was placed at 10-millimeters depth inside of the specimen is around 1.7 cm² that is around 80 percent less than the actual size of the defect. By using these data, we could come up with a system to figure out the accuracy of the results in thermal images which we called percentage of accuracy (POA). As the depth of which the defect inside the specimen increases, the amount of the POA decreases drastically.

The heat transfer simulation results provide us with a good method to refine our experimental settings. With a set of accurate material parameters, we are able to predict the experimental tests under a controlled laboratory environment. The proposed IRT method has been validated to be a good alternative to inspect concrete pavements.

References

- Allport J. et al. 1988. Quantitative Evaluation of Transient Video Thermography. In Review of Progress in Quantitative Non-destructive Evaluation, Thompson, D.O. and Chimenti, D.E. (eds), 253-262.
- ASTM. 2014. *Standard Test Method for Detecting Delamination in Bridge Decks Using Infrared Thermography*. ASTM Designation D4788-03 ed. ASTM International. West Conshohocken. Doi: 10.1520/D4788-03R13.2. ASTM
- Cannas B. et al. 2012. Modeling of Active Infrared Thermography for Defect Detection in Concrete Structures. COMSOL Conference, 1-7.
- Cielo P. et al. 1987. Thermographic Nondestructive Evaluation of Industrial Materials and Structures. 452-460.
- Clark M. R. et al. 2003. Application of Infrared Thermography to the Non-destructive Testing of Concrete and Masonry Bridges. NDT&E International. 265-275

- Gerlich V. et al. 2013. COMSOL Multiphysics Validation as Simulation Software for Heat Transfer Calculation in Buildings: Building Simulation Software Validation. 2003-2012
- Harishkumar S. et al. 2014. *Detection of Hot Spots by Thermal Imaging to Protect Power Equipments*. International Journal of Students' Research Technology & Management. 64-66
- Hiasa Sh. et al. 2016. Infrared Thermography for Civil Structural Assessment: Demonstrations with Laboratory and Field Studies. J Civil Struct Health Monit, 619-636.
- Ibarra-Castanedo C. et al. 2004. *Infrared Image Processing and Data Analysis*. Infrared Physics & Technology. 75-83
- Kruse P. W. 2001. *Uncooled Thermal Imaging: Arrays, Systems and Applications*. SPIE PRESS.
- Maldague. X. P.V. 2001. *Theory and Practice of Infrared Technology for Nondestructive Testing*. John Wiley and Sons, Inc.
- Mignogna R.B. and Green Jr. 1981. Thermographic Investigation of High-power Ultrasound Heating in materials. Ultrasonics. 159-163
- Osiander R. et al. 1998. Thermal Inspection of SiC/SiC Ceramic Matrix Composites. 339-349.
- Rajic N. 2002. Principal Component Thermography for Flaw Contrast Enhancement and Flaw Depth Characterization in Composite Structures. Aeronautical and Maritime Research Laboratory, Defense Science and Technology Organization. 521-528.
- Richter R. et al. 2012. Numerical Method of Active Thermography for Reconstruction of Back Wall Geometry. NDT&E International. 189-197
- Roche J. M. et al. 2013. Passive and Active Thermography for In-situ Damage Monitoring in Woven Composites During Mechanical Testing. AIP Conference Proceedings.
- Russ J. C. & Neal F. B. (2016). *The Image Processing Handbook*. CRC Press.

- Titman. D. J. 2001. Application of Thermography in Non-destructive Testing of Structures. NDT&E International. 149-154.
- Vavilov V. P. & Taylor R. 1982. Theoretical and Practical Aspects of the Thermal Non-destructive Testing of Bonded Structures. Research Techniques in NDT. 239-279.
- Vollmer M. & Möllmann K-P. 2011. Infrared Thermal Imaging: Fundamentals, Research and Applications. John Wiley & Sons.
- Watase A. et al. 2015. Practical Identification of Favorable Time Windows for Infrared Thermography for Concrete Bridge Evaluation. Construction and Building Materials, 1016-1029.
- Wu D. et al. 1997. *Phase-sensitive Modulation Thermography and its Applications for NDE*. Conference on Thermal Sensing and Imaging Diagnostic Applications.

CHAPTER THREE: A REAL-TIME THERMAL IMAGING-BASED SYSTEM FOR
ASPHALT PAVEMENT SURFACE DISTRESSES INSPECTION AND 3D CRACK
PROFILING

Aidin J. Golrokh^I, Dr. Yang Lu^{II} and Dr. Xinyu Gu^{III}

I: Graduate research assistant at Boise State University

II: Associate professor at Boise State University

III: Professor at Southeast University

Abstract

Infrared thermography is an effective nondestructive testing approach to assess surface and near surface distresses, such as asphalt pavement surface cracks. However, the raw data from thermal cameras is not sufficient for pavement surface distress inspection. The objective of this research is to develop an integrated new system that combines infrared imaging, high resolution visible light imaging, real-time image processing, and data-rich analytics for automated inspection. The developed system features collecting frames from both thermal and visual images and then aligns them together for further data processing to support pavement preservative maintenance decisions. The developed system can correlate the temperature data with the profile of cracks including both width and depth. We developed an algorithm that can integrate the characteristics captured by both thermal and visual images to provide a quantitative identification of the location of surface cracks and their severity. Field testing data has been collected and a model-based statistical analysis was conducted to identify a

correlation between the temperature gradient and the surface crack profile on asphalt pavements. A correlation between the temperature that is collected using infrared thermography and the depth of the crack has been established with a fair accuracy using regression analysis. This work can provide fast and easy decision support to improve pavement preservation practices by identifying the severity of the crack using only infrared thermography data that is collected from the surface of the pavement.

Keywords: Infrared thermography; Asphalt pavements; Surface cracks; ANOVA; Regression test

Introduction

Non-destructive tests (NDT) such as ground penetration radar (GPR), ultrasonic test (UT) and infrared thermography (IRT) have become a common means of assessment for defects of roadway pavements and structures. Among these, GPR and UT methods are mostly used for detecting subsurface defects inside asphalt domains and investigating the thickness of such pavements (Bastard et al. 2007, Szymanik et al. 2016). IRT has proven to be more effective for investigating close-to-surface delamination and surface cracks (Lu et al. 2017). The accuracy of these tests along with the ease of their use eliminates the time and expenses that should be spent when using traditional forms of pavement tests such as chain dragging and hammer sounding (Vaghefi et al. 2011).

In this paper, IRT is used as a NDT tool to augment the reliability of asphalt pavement assessment. A correlation between the temperature variance of the crack and its profile is studied. This will help to predict the severity of the pavement surface cracking and delamination by using the thermal data that are obtained from IRT. IRT monitors surface radiations of electromagnetic waves, in the infrared wavelength, related to

temperature gradient between the sound and delaminated areas (Watase et al. 2015).

There are some advantages in favor of using IRT for inspecting roadways and bridges for delamination detection compared to other means of NDT. One of the advantages of IRT is that it does not need immediate access to the surface of its target. This allows the inspectors to be able to apply IRT on the surface of the roadways and bridges with a speed of 16 km/h (10 mph), (ASTM 2014), which makes it a favorable NDT method used for surface investigations of such structures with less interference with ongoing traffic compared to other NDT methods (Hiasa et al. 2016).

In contrary to all of these benefits regarding IRT, there are some obstacles that need careful consideration before implementing IRT in order to avoid effecting the results. Results gathered from IRT can be affected by factors related to camera specifications and environmental conditions. These factors are mostly related to the speed of the data collection, time window of the day in which IRT is applied, weather conditions, ambient temperature inconsistencies, angles in which images are taken and other variables. Hiasa and his colleagues (Hiasa et al. 2016) have distinctly covered different types of IRT approaches in their studies. They stated that these effective factors should be kept constant when thermography is applied in order to be able to compare measurements which demonstrate the defects on target structures.

Among the different types of IRT that Hiasa and colleagues (Hiasa et al. 2016) have covered in their publications, there are two types of IRT for investigating asphalt domains which are called passive and active IRT. In a passive approach on structures such as bridge decks, natural sources of heat which are present in the environment surrounding the target, such as solar radiation and ambient temperature, are used to heat

up the surface of the specimen. These sources are the direct cause for the thermal excitation of the domain (Milovanovic and Pecur 2016). In an active approach however, heat generators such as hot air blowers, microwaves, electricity or vibrations are used to employ heat on the surface or the body of the domain (Kashif Ur-Rehman et al. 2016). In this paper passive IRT is used to inspect asphalt pavement surface on the field.

Pavement Surface Thermal Field

Both active and passive IRT processes rely on the temperature gradient of the surface of the target. This gradient is caused by the back and forth bouncing of the sunlight inside the crack, which eventually heats up the walls of the crack and makes the temperature elevate, as shown in Figure 3-1 (Sham et al. 2008).

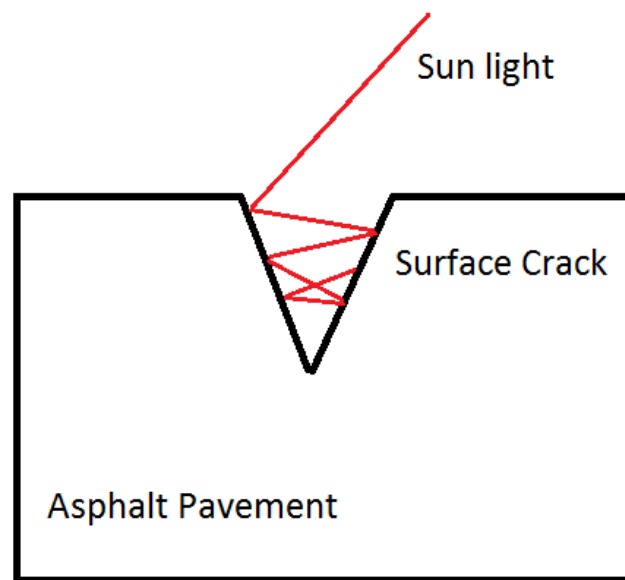


Figure 3- 1. Surface delamination temperature gradient

These temperature gradients are useful features which have become the basis for the IRT approach of nondestructive testing of civil pavements and structures. This phenomenon will be used in this paper to classify different types of cracks on top of

asphalt pavements and to correlate temperature distribution of the crack to its width and depth.

IRT Mechanisms

As mentioned earlier, IRT is based on the temperature gradient of the surface of the target. This temperature gradient is caused by one of the modes in which heat can be transferred throughout the domain, which are heat conduction, heat convection and heat radiation. IR thermal cameras, in particular, sense and measure the radiative heat flow from the target (Kaplan 2007). The amount for thermal radiation emitted from the surface of the target depends on its emissivity. Emissivity is defined as the ratio of the energy radiated from a material's surface to that radiated from a blackbody that is considered as a perfect emitter, with emissivity equal to 1 (Minkina and Dudzik 2009). All warm objects radiate energy that is in the infrared zone of the electromagnetic spectrum which can be measured by infrared thermal cameras and then converted into temperature values by using the following governor equation known as the Stephan Boltzmann law (Starnes et al. 2003):

$$W = \epsilon \sigma T^4 \quad (3-1)$$

In this equation, W is radiant flux emitted per unit area (watts/m²), ϵ is emissivity value of the domain (unitless), σ is Stephan-Boltzmann constant equal to 5.67×10^{-8} (watts/m²/k⁴) and T is the absolute temperature of the domain in Kelvins.

As is shown in the Equation 3-1, emissivity is an effective factor in calculating emitted radiant flux and it is a number between 0 (perfect reflector) to 1 (perfect emitter). For both concrete and asphalt this number is fixed, depending on their specifications, and is close to 1. Unless there is moisture on the surface of our targets in the pavement field, there will be no shortcoming related to emissivity when it comes to inspecting asphalt pavements by using IRT.

Thermal cameras will measure W and then by using equation 1, it will calculate the temperature and assign it to each pixel of the image. We can identify anomalies using IRT by reading the temperature gradient between the sound and delaminated areas using the following equation (Hiasa 2016):

$$\Delta T = T_d - T_s \quad (3-2)$$

T_d is the temperature recorded at the delaminated area, T_s is the temperature recorded at the sound area and ΔT is the temperature gradient.

Another equation called Wien's displacement law is used to choose the right thermal camera for a specific target. As can be seen in the following equation, this law relates the surface temperature of the target to the maximum wavelength of the energy that is emitted from it (Watase et al. 2015):

$$\lambda_m = \frac{b}{T} \quad (3-3)$$

λ_m is the wavelength of maximum radiation (μm), b is Wien's displacement constant equal to 2897 ($\mu\text{m}/\text{K}$) and T is absolute temperature of the target (K). Depending on the wavelength of radiation and the maximum and minimum temperatures that are going to be felt on the target, an appropriate thermal camera, that captures all the invisible wavelengths, can be chosen to read corresponding temperatures (Kaplan 2007).

IRT Time Window

A very important aspect of using passive IRT is to choose the best time window during the day for collecting thermal data. For surface and subsurface evaluation of pavement anomalies there are different recommended time windows according to several other sources. Washer et al. (2009) recommended, depending on the depth in which the defect is located, 5 to 9 hours after sunrise to conduct IRT. Gucunski et al. (2013), on the

other hand, mentioned that a thermal image that was taken 40 minutes after sunrise gave clearer results compared to a thermal image that was taken at noon. A third recommendation provided by Kee et al. (2012), concluded that delamination that is located around or deeper than 6.4 centimeters inside the body of the target will not be detected at around 3 hours and 45 minutes after sunrise. Watase et al. (2015) compares the time window to the location of delamination on bridges. For example, according to this approach, Noon is favorable for the top of the deck and midnight for the soffit of the deck. Hiasa (2016) also considers the midnight cooling effect as a preferable time window for thermal imagery of bridge decks. In our research, most of the thermal data were collected within 2 hours prior to sunset in which the cracked and sound areas of the pavements had the highest temperature contrast. During this period, there was no direct sun light on top of the surface that was being investigated. Therefore, it can be assumed that the collected images were not affected by excessive solar radiation.

Statistical Approaches

This research consists of two major aspects, which are the collection of data and the study of the significance of those data. Statistical approaches are employed in order to compare the data and evaluate a trend line that can relate the crack temperature to its profile.

Analysis of Variance Test

The temperature data are collected into three groups and each group has similar conditions, such as ambient air temperature, weather condition, and other effective factors. The analysis of variance (ANOVA) model is used to determine the homogeneity of these data sets. The ANOVA model determines whether there is a significant statistical

difference between the means of three or more groups of data. It is worthy to mention that variance is the square of standard deviation. Even though standard deviation is more comprehensible, variance is more widely used in statistical analysis (Parchami et al. 2017). On the other hand, the null hypothesis is a regularly used term in ANOVA models, which is a general statement that there is no relationship between two measured phenomena or no possible association among different groups (Everitt 1998). In other words, the null hypothesis confirms that the probability of a major difference between the means of different groups of data is not significant.

The significance level, denoted as α , is the probability to reject the null hypothesis. In this study a significance level of 0.05 is chosen which means there is 5% risk that a significant difference exists where it is assumed there is no actual difference (Frost 2015). The significance level of 0.05 is widely used in academic research (Guan 2011).

An ANOVA test statistic is the variance ratio (V.R.), also known as F-value, with appropriate amounts for numerator degrees of freedom (DOF) and denominator DOF. Numerator DOF is the degrees of freedom of the model which contains the data groups. Denominator DOF is the degrees of freedom of the error at a chosen α . In this case $\alpha = 0.05$. Note that the DOFs of numerator and denominator and also α , will be used to calculate the critical amounts for F inside the ANOVA table as shown in Table 3-1. This concept will be mentioned with more details inside the results and analysis section.

The following table, known as an ANOVA table, contains all the equations needed to construct V.R. The summation of data points ($\sum x$), summation of squares ($\sum x^2$) and number of data points (n) should be calculated for each individual group

before constructing the following table. These values will be used to compute components of the ANOVA table. The table contains three sources of variation in the data, which includes total, group and error.

Table 3- 1. ANOVA table of equations

Source	df	SS	MS	F
Total	N-1	[B]	-	-
Group	k-1	[C]	[E]	[G]
Error	N-k	[D]	[F]	

In this table, df is the degrees of freedom in each source, SS is the sum of squares due to the source, MS is the mean of sum of squares due to the source and F is variance ratio (F-value). In addition, N is denoted as the total number of measurements, k is the total number of groups. Therefore, k-1 is considered as the numerator DOF and N-k is considered as the denominator DOF.

The equations in the table are as follows: [A] is $CF = \frac{(\sum x)^2}{N}$ where CF is the correction factor, [B] is $SS_{Total} = Sx^2 - CF$ and [C] is $SS_{Group} = \sum \frac{(\sum x)^2}{N} - CF$. [D] is $SS_{Error} = SS_{Total} - SS_{Group}$, [E] is $MS_{Group} = \frac{SS_{Group}}{df_{Error}}$ and [F] is $MS_{Error} = \frac{SS_{Error}}{df_{Error}}$. The final product of the ANOVA table is [G] which is $V.R. = \frac{MS_{Group}}{MS_{Error}}$.

Another entity that is calculated for this ANOVA study is the P-value. P-value is the probability of having more extreme value of F-value compared to what is calculated in a specific case under the null hypothesis. This entity can help to decide the amount used for α in the ANOVA study.

For calculating the variables of this table including F-value, an ANOVA code is employed in statistics software R and R commander (Fox et al. 2009).

Regression Test

A regression test is a statistical model that estimates a potential relationship among different variables using statistical processes. Curve or data fitting is the process, which builds up a curve, or mathematical function, which fits well with our data in our data set (Halli and Rao 1992). The objective of using a regression test in this paper is to study the existence of any correlation between the profile of the crack, such as its depth and width, with the temperature that is collected from the same data points using a thermal camera. By using a MATLAB code for the data fitting process, this correlation was studied and a trend line was drawn.

Experimental Methodology

In this section different aspects of the experiment are going to be discussed and the experimental procedure is going to be laid out.

Crack Profile Data Collection

Width and depth, as two of the major components of crack profile, are two of the effective factors on the temperature gradient which is present within a pavement delaminated surface. Figure 2 illustrates how width and depth of the crack are measured in the field. The width is considered as the distance between the two edges of the opening mouth of the crack. The depth is the measurement of the distance between the top edges of the crack to the lowest section of it.

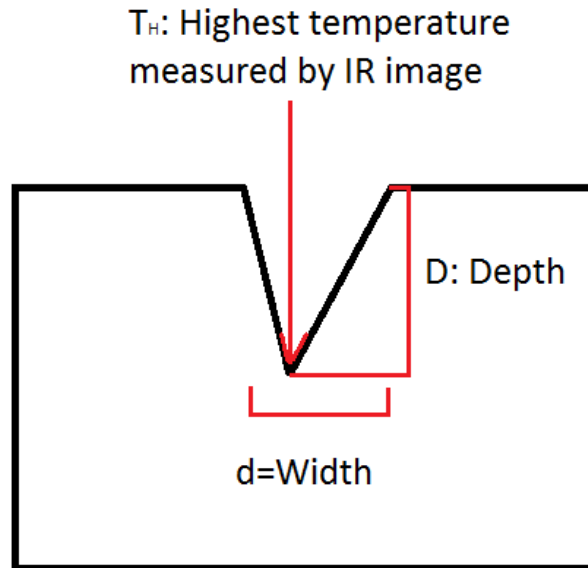


Figure 3- 2. Correlation between depth and width and temperature

IR Thermal Image Collection

In order to locate the delaminated areas on top of the asphalt domain by capturing the temperature gradient on the surface, the raw collected image data must be processed using a processing algorithm which will be discussed in the next section of this paper. This processed image consists of a visual image and a thermal image which have been aligned on top of each other in the post-processing section of the research. The camera setup which can capture both thermal and visual images simultaneously is shown in Figure 3-3.



Figure 3-3. Mobile thermography testing setup

IRT processing algorithm

In the following, the premise of the processing algorithm will be discussed and the employment of the algorithm on each frame that was collected using the camera setup will be fully explained. In Figure 3-4, the visual and thermal frames that are collected from the surface of the road are shown. These images were taken on a relatively hot day from the surface of a sidewalk.

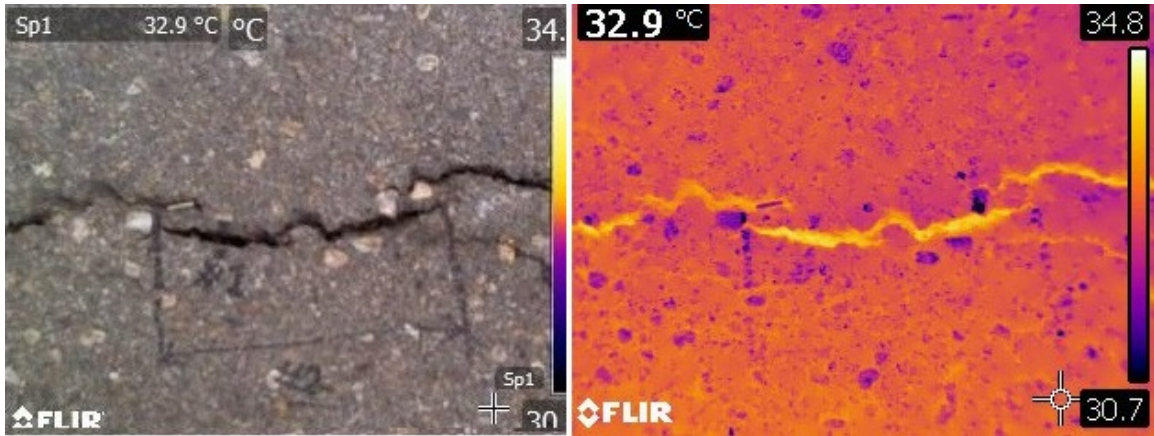


Figure 3- 4. Visual versus thermal images

The minimum temperature in the thermal image (shown in Figure 3-4) is around 31 degrees Celsius and the maximum temperature is around 35 degrees Celsius. In order to be able to apply the processing algorithm, the colored image is converted to a grayscale image. The colored image is called RGB image since the majority of the colors in the image that are perceivable by humans are constructed from primary spectral components of red, green and blue (Kumar and Verma 2010). A simple way to convert RGB image to grayscale image is to take the average of the base colors as shown in the following equation:

$$I = \frac{R+G+B}{3} \quad (3-4)$$

In this equation, I is the intensity function and R, G and B are the intensities for red, green and blue respectively.

Since humans do not perceive the main colors equally, a simple averaging method of the three main colors is not accurate. Therefore, a more precise conversion method will weigh colors based on how the human eye perceives them. This method is known as the Luminosity Method and is used in this paper as the algorithm for converting RGB image to grayscale image. The Luminosity Method is a sophisticated version of the average

method which assigns different weights to each color based on humans' perception of that color (Cook 2009). For instance, in this algorithm, since humans are more sensitive to green than other colors, more weight is assigned to green. The following equation is used to transform the colored image into grayscale image:

$$I_y = 0.2989R + 0.5870G + 0.1140B \quad (3-5)$$

The coefficients in this equation are empirically derived from a series of trichromatic color matching experiments by previous authors (Wright 1928, Guild 1930, Fairman et al. 1997).

The Luminosity Method is a transition between the raw thermal image (Figure 3-4) and the processed image (Figure 3-5). During this transition, colored images are converted into grayscale images. Later on, a number of thresholds, known as gray thresholds, will be assigned to these grayscale images. Each image is constructed of 255 different thresholds and each of these thresholds are assigned to a specific temperature. In this image, Figure 3-4, a gray threshold corresponding to 33 degrees Celsius, is used to get the best contrast between the delaminated area and the sound area (Lu et al. 2017). By choosing this threshold, all the pixels that have a measured temperature less than the indicated corresponding temperature will be eliminated from the image (Ibarra-Castanedo 2004). Therefore, this can clarify the area of the delaminated surface for further study inside the computer (Neal 2016). Figure 3-5 shows the processed image after employment of the threshold using our developed code.



Figure 3- 5. Processed image

Test Setup and Data Collection for Passive IRT

Five locations have been selected for this study in the Boise, Idaho region. One location was on a deteriorated roadway, two locations were on the pedestrian sidewalk, another location was inside a parking lot and the last location was on a major roadway. Most of the images were taken from mid-September to mid-October. The temperature did not change drastically during this period with the exception of the last day of data collection, in which the temperature dropped significantly. The days in which thermal images were collected were mostly sunny and the locations for the most part were under direct sunlight throughout the daytime. There was no noticeable wind during the thermal image data collection and there was no moisture present on the surface of the road in any of the locations. The average recorded relative humidity was between 38 to 49 percent.

Temperature gradient of different parts of the road is one of the major obstacles when it comes to on-site thermal imagery. Different sections of the road are going to have

different temperatures assigned to them. In addition, cracks that are under the shadow of the trees or buildings will not have the same temperatures compared to the ones that have been under direct sunlight throughout the day. Another major factor that can cause temperature gradient is the time of the day. Since data has been collected during the cooling cycle, cracks tend to lose temperature rapidly. On the other hand, it is not practical to gather all the data in one day due to the limited time windows in which the thermal imagery is being applied. Since ambient air temperature varies on a daily basis depending on the time of the year in which the inspection is taking place, different temperatures will be recorded with the thermal camera.

Many previous authors have come up with different solutions to address these phenomena. For instance, Shuhei Hiasa, et al. (2017), who have done a detailed thermal investigation of concrete subsurface delamination detection using thermal imagery, brought solar radiation into consideration as the main source of heat in their on-site model. Even though solar radiation is a major factor in heating up the surface of the crack, it does not consider some of the altering factors in temperature gradient that were already mentioned.

In this research, a number of data from roadways have been gathered to address different aspects of IRT. In order to construct the crack profile, depth and width of crack is measured using a digital caliper (Figure 3-6).



Figure 3- 6. Measuring depth and width of crack using digital caliper

Different means have been used to calculate temperatures in the field. The ambient air temperature is collected from the weather information of the nearest weather station. A thermocouple is used to calculate the temperature of the bottom of the crack, as shown in Figure 3-7. This data is used to calibrate and confirm the temperature data that is collected from the thermal camera.

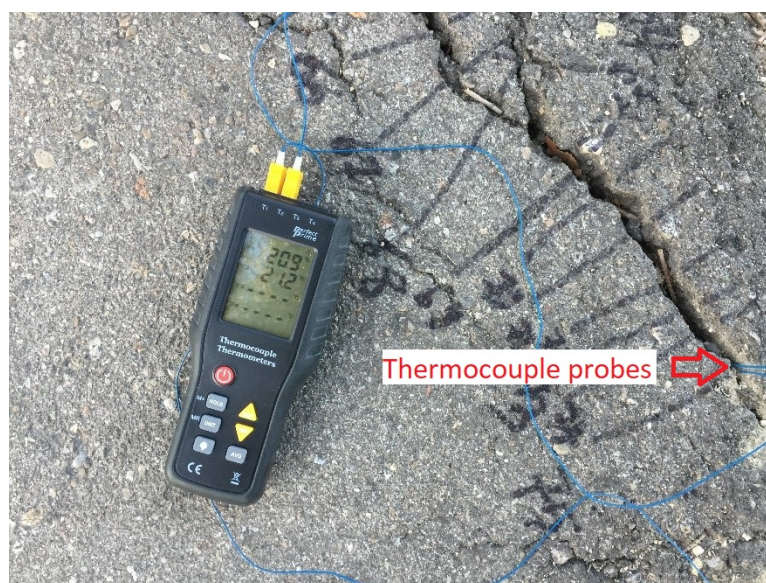


Figure 3- 7. Thermocouple is used for measuring the mean temperatures inside cracks

Thermal images for passive IRT are gathered using the setup that is introduced in the previous section of this paper. The height of the cameras is set to be around one meter

above the ground. The frames of the thermal video are processed and the data are stored for further investigation.

Results and Analysis

Statistical analyses are employed on the collected data in order to determine a correlation between the different aspects of crack profile and crack temperature. The premise of this study is to examine the possibility of comparing the width and the depth of the crack to the temperature of its deepest section. If such correlations between depth, width and corresponding temperature exist, the data gathered from the thermal images can solely be used to predict the depth of the crack without going through the process of gathering field measurements. In other words, the severity of the defective areas of the road can be predicted by using the recorded thermal images.

As mentioned in an earlier section, the ANOVA method has been used to study the relationship between the means of the temperatures that have been collected during different days and under different weather conditions. There are three groups of data available that contain temperature data points that were collected under similar circumstances during the span of two months. These circumstances include, but are not limited to, similar ambient air temperatures and weather conditions. The following box plot shows the result of the ANOVA study for these three groups.

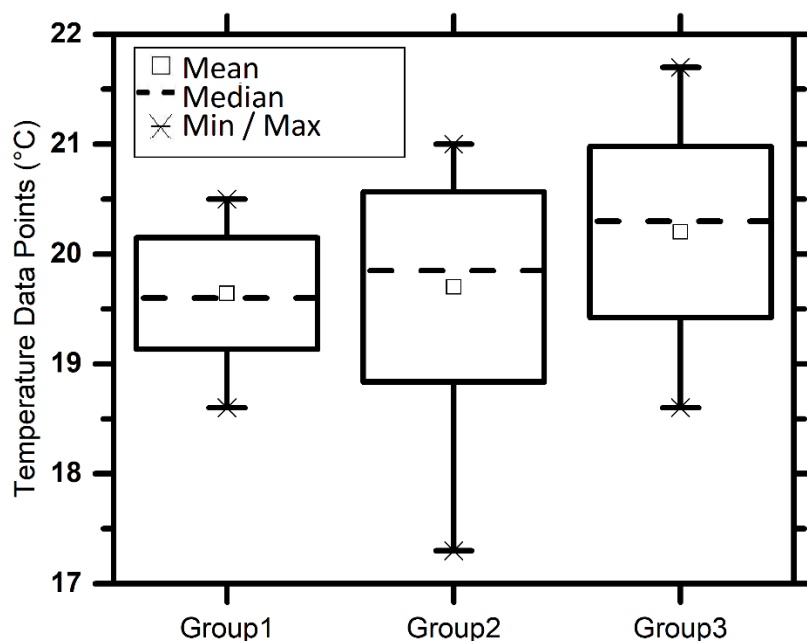


Figure 3- 8. Boxplot of temperature data points which are separated into three groups with similar ambient air temperatures and weather conditions

As is shown in Figure 3-8, the lowest temperature that is recorded on the field belongs to the second group, which is close to 17 degrees Celsius, and the highest temperature belongs to the third group, which is close to 22 degrees Celsius. On the other hand, the means of the temperatures belonging to each group set are located between 19.5 to 20.5 degrees Celsius.

Tables 3-2 through 3-4 show the final results of the ANOVA study. Each entity in these tables has been introduced in the statistical approaches section, please refer to Table 3-1. In Table 3-4, F is the variance ratio which will be used to conclude whether the null hypothesis is rejected in this ANOVA study.

Table 3- 2. Preliminary results based on three groups of temperature data points

Σx	589.2	591	604.5
$(\Sigma x)^2$	347156.64	349281	365420.3
$(\Sigma x)^2/n$	11571.888	11642.7	12180.68
Σx^2	11579.36	11664.42	12198.03
n	30	30	30

Table 3- 3. Total number of measurements, total number of groups and correction factor

N	90
k	3
CF	35390.601

Table 3- 4. ANOVA table

Source	df	SS	MS
Total	89	51.209	NA*
Group	2	4.662	2.331
Error	87	46.547	0.535023

NA: Not applicable

It is calculated from Table 3-3 that the F value for the three groups of data points is equal to 4.356822. This number shows an exact match to what is calculated using the existing ANOVA model in R software which is 4.357. Furthermore, the calculated P-value from Table 3-3 is 0.0157. Since the amount of P-value is more than 0.01, an α equal to 0.05 is going to be used to study the null hypothesis. In addition, it is calculated that the numerator DOF of the F value is 2 and denominator DOF of the F value is 87 as shown in the table. From the F distribution table with $\alpha = 0.05$, it is found that $F_{2,87}=3.1$. Since the calculated F value is higher than this amount, the null hypothesis is rejected. This indicates that there is distinguishable difference between the means of data sets. In other words, the difference in the means of the three groups is statistically significant. Therefore, it is proven that ambient temperature gradient and weather conditions of different days of the data collection period are effective on the temperature of the cracks.

In the following, regression method is used to illustrate the effect of this difference between the means of the data sets on a comparison study that is conducted between the temperature of the crack and its depth. In Figure 3-9, a graph of crack depths versus corresponding temperatures of the crack are plotted and a trend line is measured

using a regression test. As is shown in this graph, the minimum temperature that is recorded from the field is 18.4 degrees Celsius and the maximum temperature is 21.7 degrees Celsius. The depth of cracks vary from 1.1 millimeters up to 47.4 millimeters and the majority of the depth measurements are between 1 to 10 millimeters. The adjusted R^2 for this line, which is a representation of the coefficient of determination, is close to 35%. This indicates that the trend line that is correlating the depths and temperatures of the cracks has a relatively low accuracy.

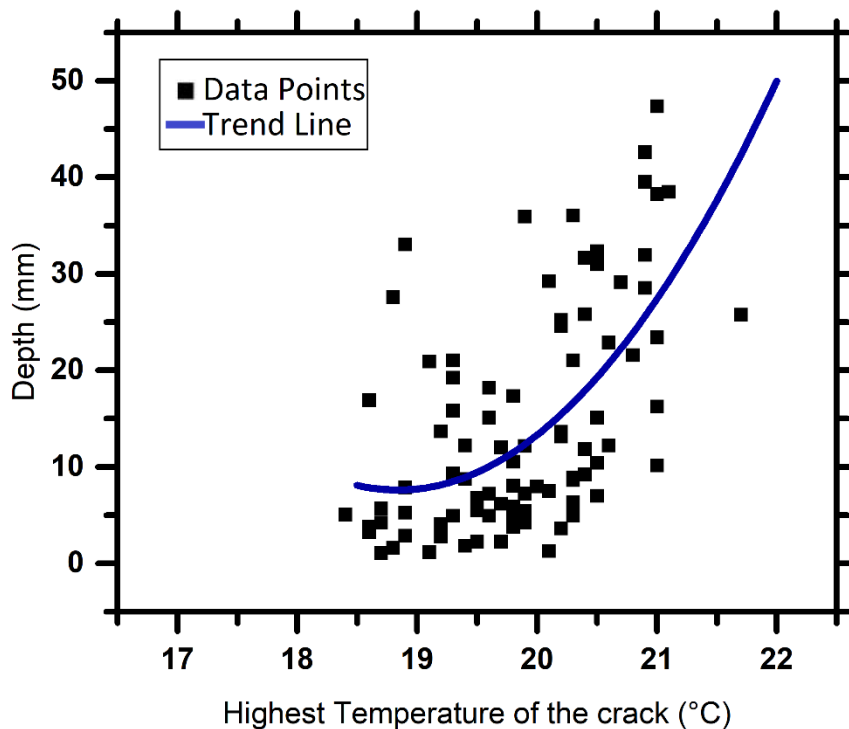


Figure 3- 9. Relationship between depth and the highest temperature that is recorded from the crack

In order to minimize the effect of surrounding factors, such as ambient air temperature, and to improve the prediction capacity of the crack parameters by using the temperature data, the authors present a unique approach. The term point-wise

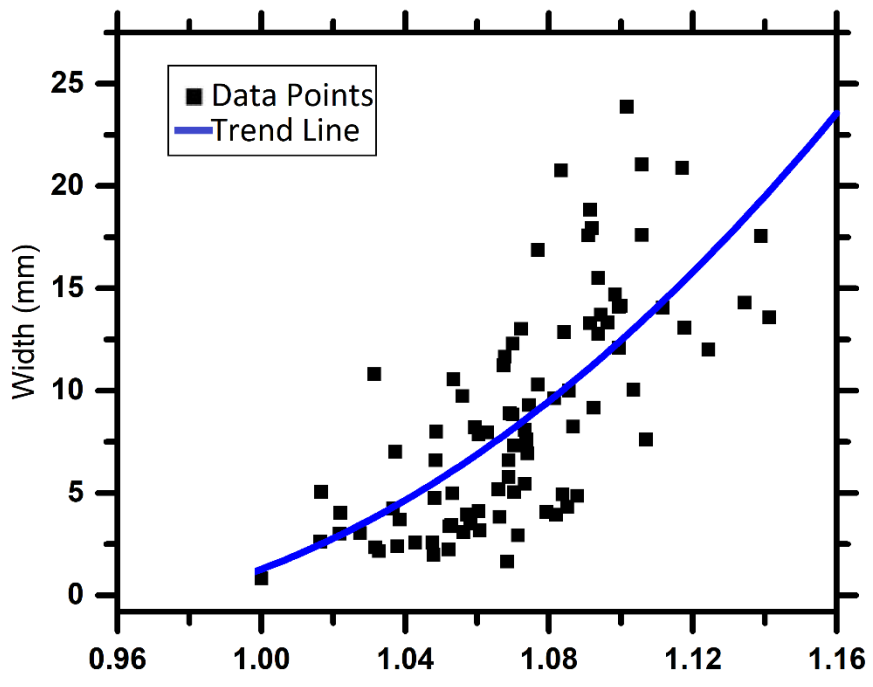
normalization method is used for this approach. By using this method, the temperature data is normalized pixel by pixel using another factor, which is calculated from the information of the thermal image, to construct a unitless entity. This factor can also be calculated from the field measurements. In point-wise normalization method a virtual rectangular box is considered around each pixel located on the cracked area shown in the thermal image from Figure 3-10. The temperature data of the sound area are collected from each corner point of this box. The averages of the collected temperatures on each of these boxes are calculated and used to normalize the temperature of the crack at that point. The box contains points on its corners which in most of the cases are located on sound parts around the crack. As shown in Figure 3-10, the sizes of the boxes are identical and the deepest part of the crack is located in the middle of each box. The calculated average temperature of this box is called the average ambient surface temperature and is used to normalize the temperature data of the cracked area using the following equation:

$$\text{Point-wise normalized temperature} = \frac{\text{Individual crack temperature}}{\text{Average of ambient surface temperature}} \quad (3-6)$$



Figure 3- 10. Calculation of the average ambient surface temperature

The point-wise normalized temperature was first compared with the measured width of each data point on cracks as shown in Figure 3-11. The correlation between the two entities is illustrated in this figure. The minimum point-wise normalized temperature is calculated to be 1 and the maximum point-wise normalized temperature is calculated to be 1.14. The minimum point-wise normalized temperature will never become less than 1 as it is clearly shown in the graph. This is because the temperature of the crack is equal or higher than the temperature of the surrounding sound area during the cooling cycle. The width of cracks varies from 0.85 millimeters up to 24 millimeters. A correlation can be observed between widths and point-wise normalized temperatures but the adjusted coefficient of determination (R^2) for this trend line, which is equivalent to its accuracy, is around 50 percent. This means that the data points are relatively scattered in this correlation study.



Point-wise normalized temperature based on ambient surface temperature

Figure 3- 11. Relationship between width and point-wise normalized temperature based on average ambient surface temperature

In another attempt, the depth as the second measured parameter of the crack profile was compared with the point-wise normalized temperature, which is plotted in a graph, and a trend line is calculated to represent the data set (Figure 3-12).

Higher and lower band lines indicate the data range in which the depth measurements are located in. Each individual point-wise temperature can be related to a specific range of depth measurements. For instance, 1.04 represents a range of measured depths between 1 to 6 millimeters while 1.12 represents a range of measure depths between 25 to 40 millimeters. This clearly shows that as the point-wise normalized temperature rises the length of the measured depth also increases.

The corresponding equation for this trend line is $Y=2193X^2-4375X+2182$ and the adjusted coefficient of determination (R^2) for this trend line is 70.06%. In this equation Y represents the depth and X represents the point-wise normalized temperature of each data point on the crack. This trend line is a more accurate representation of the data and shows that as the temperature of the crack, with respect to the ambient surface temperature, increases then the depth of the crack also increases. After plotting the trend line, it is possible to calculate the original temperature by multiplying the point-wise normalized temperature with the mean ambient surface temperature. Therefore, it is reliable to connect each measured temperature of the crack to its corresponding depth data.

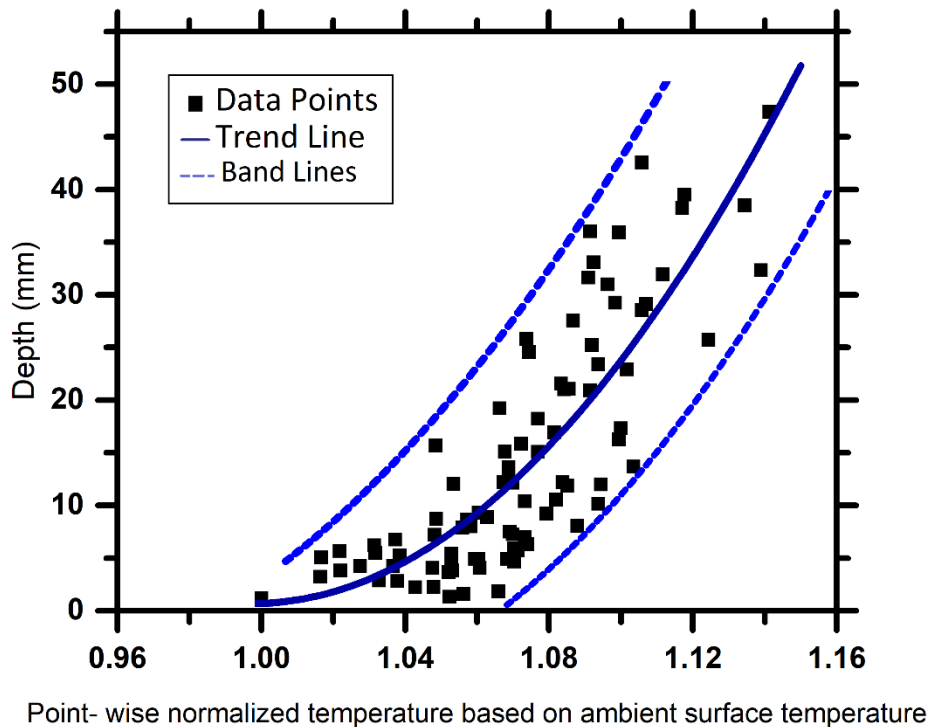


Figure 3- 12. Relationship between depth and normalized temperature based on average ambient surface temperature

Conclusion

In this study, a correlation between the temperature gradient related to the surface crack of asphalt pavement and its profile has been studied.

1. A portable real-time IRT system is developed. In this developed system, thermal and visual videos of the pavement surface are combined and then segmented into image frames. Each frame is processed by precisely aligning thermal and visible light images for surface crack detection based on temperature gradient, which shows on the deteriorated asphalt pavement surface.

2. Two sets of pavement data (surface temperature and crack profile) were collected on-site from the field. The first data set was the temperature map collected using the proposed IRT inspection system. The second data set was the measured depth and width of the crack at identified data points using a digital caliper.

3. A series of statistical studies have been conducted on the collected data to see the correlation between each aspect of crack with the temperature gradient. The ANOVA model is a feasible tool to determine whether there is a significant statistical difference between the means of three or more data sets. In this case, the calculated variance ratio was around 4.357, which rejected null hypothesis. This indicates that distinguishable difference is present between the means of the different temperature data set groups. Therefore, to mitigate the effect of this difference, a unique approach, named point-wise temperature normalization, is developed by the authors. Temperatures were normalized based on the mean temperature of the sound area around each data point. A unitless representation of temperature was calculated and compared with depth and width measurements.

By achieving a 70 % reliability, a correlation between point-wise normalized temperature and crack depth was established using regression method. This method can be used to determine the severity of the surface deterioration based on thermal imaging data collected from the surface of the asphalt pavements. It has been validated that the developed IRT inspection system can be used to investigate the severity of pavement by correlating the temperature gradient to the severity of the deterioration. This developed system can provide decision support to improve pavement preservation practices.

References

- ASTM 2014. *Standard Test Method for Detecting Delamination in Bridge Decks Using Infrared Thermography*. In Proceedings of the ASTM Designation D4788-03 ed. ASTM International, West Conshohocken, Penn, USA.
- Bastard C.L., Baltazart V., Wang Y., Saillard J. 2007. *Thin-pavement thickness estimation using GPR with high-resolution and superresolution methods*. IEEE TRANSACTIONS ON GEOSCIENCE AND REMOTE SENSING, 2511-2519.
- Cook J. D. 2009. *Three algorithms for converting color to grayscale*. <https://www.johndcook.com/blog/services-2/>.
- Everitt B. 1998. *The Cambridge dictionary of statistics*. Cambridge University Press.
- Fairman H. S., Brill M. H., Hemmendinger H. 1997. How the CIE 1931 color matching functions were derived from Wright-Guild data. *Color Res Appl*, 11-23.
- Fox J., Andronic L., Boye T., Calza, S., Wolf P. 2009. *Rcmdr: R commander (Version 1.6-3)*. Software is available from <http://CRAN.R-project.org/package=Rcmdr>.
- Frost J. 2015. Understanding hypothesis tests: Significance levels (Alpha) and P Values in statistics. <http://blog.minitab.com>.
- Guan K. K. 2011. Surface and ambient air temperatures associated with different ground material: a case study at the University of California, Berkeley. *Surface and Air Temperatures of Ground Material*, 1-14.

- Gucunski G., Nazarian S., Yuan D., Kutrubes D. 2013. *Nondestructive testing to identify concrete bridge deck deterioration*. Transportation Research Board, SHRP 2 Report S2-R06A-PR-1, Washington, DC.
- Guild J. 1930. *The colorimetric properties of the spectrum*. Philos. Trans. Roy. London, Ser. A, 149-187.
- Halli S.S. & Rao K. V. 1992. *Advanced Techniques of Population Analysis*.
- Hiasa S. 2016. *Investigation of infrared thermography for subsurface damage detection of concrete structures*. Doctoral Dissertation (Open Access).
- Hiasa S., Birgul R., Catbas F.N. 2016. *Infrared thermography for civil structural assessment: demonstrations with laboratory and field studies*. Journal of Civil Structural Health Monitoring, vol. 6, no. 3, pp. 619–636.
- Hiasa S., Birgul R., Catbas F. 2017. *Effect of defect size on subsurface defect detectability and defect depth estimation for concrete structures by infrared thermography*. J Nondestruct Eval, 1-21.
- Ibarra-Castanedo C. 2004. *Infrared Image Processing and Data Analysis*. Infrared Physics & Technology, 75-83.
- Kaplan H. 2007. *Practical applications of infrared thermal sensing and imaging equipment*. Third edition.
- Kashif Ur-Rehman S., Ibrahim Z., Memon S.A., Jameel M. 2016. *Nondestructive test methods for concrete bridges. A review*. Constr. Build. Mater. 107. 58-86.
- Kee S., -H., Oh T., Popovics J.S., Arndt R.W., Zhu J. 2012. *Nondestructive bridge deck testing with air-coupled impact-echo and infrared thermography*. J. Bridge. Eng. 17, 928-939.
- Kumar T. & Verma K. 2010 *A Theory on Conversion of RGB image to Gray image*. International Journal of Computer Applications (0975 - 8887), 7-10.
- Lu Y., Golrokh A.J., Islam M.A. 2017. *Concrete pavement service condition assessment using infrared termography*. Hindawi publications, 1-8.

- Milovanovic B. & Pecur I.B. 2016. Review of active IR thermography for detection and characterization of defects in reinforced concrete. *Journal of Imaging*, 1-27.
- Minkina W. & Dudzik S. 2009. *Infrared thermography: Errors and uncertainties*. John Wiley and Sons Ltd, The Atrium, Southern Gate, Chichester, West Sussex. PO1985Q, United Kingdom.
- Neal J.C. 2016. *The Image Processing Handbook*. CRC Press.
- Parchami A, Nourbakhsh M., Mashinchi M. 2017. *Analysis of variance in uncertain environments*. Springer Heidelberg, 189-196.
- Sham F C., Chen N., Long L. 2008. *Surface crack detection by flash thermography on concrete surface*. The British Institute of Non-Destructive Testing.
- Starnes M.A., Carino N.J., Kausel E.A. 2003. Preliminary thermography studies for quality control of concrete structures strengthened with fiber-reinforced polymer composites. *J. Mater. Civ. Eng.* 15, 266-733.
- Szymanik B., Frankowski P.K., Chady T., Robinson C. Chelliah A.J. 2016. Detection and inspection of steel bars in reinforced concrete structures using active infrared thermography with microwave excitation and eddy current sensors. *MDPI*, 1-16.
- Vaghefi Kh., Silva, H., Harris, D., Ahlborn Th. 2011. Application of thermal IR Imagery for concrete bridge inspection.
- Washer G., Fenwick R., Bolleni N. 2009. *Development of hand-held thermographic inspection technologies*. report No. OR10-007.
- Watase A., Birgul R., Hiasa S., Matsumoto M., Mitani K., Catbas F. N. 2015. *Practical identification of favorable time windows for infrared thermography for concrete bridge evaluation*. *Construction and Building Materials*, 1016-1030.
- Wright W. D. 1928-29. A re-determinaion of the trichromatic coefficients of the spectral colours. *Trans. Opt. Soc. London*, 141-164.

CHAPTER FOUR: A FULL-SCALE EXPERIMENTAL STUDY OF THE EFFECTS
OF DIFFERENT CLIMATE CONDITIONS ON INFRARED THERMOGRAPHY AND
SURFACE DELAMINATION ASSESSMENT IN CONCRETE STRUCTURES

Aidin J. Golrokh^I and Dr. Yang Lu^{II}

I: Graduate research assistant at Boise State University

II: Associate professor at Boise State University

Abstract

There is a growing interest in using non-destructive testing methods to inspect bridges, road pavements and other civil structures. Infrared thermography is considered one of the most effective NDT methods for surface and close-to-surface defect assessment on concrete pavements and structures. Thermography is used to correlate the temperature gradient that is present on the delaminated concrete surface to the defect profile. At the same time, the method is more affected by ambient air conditions compared to other methods of non-destructive testing. In this paper, a new testing system is presented to study and evaluate environmental effects of thermography and temperature reading of thermal cameras. The effects of wind speed and level of humidity on the performance of the camera are also studied in depth. It can be concluded from the findings of this paper that both humidity and wind can have major effects on thermography and its use for detecting surface distress. It is also found that the effect of wind is significantly greater than humidity on thermography for different crack profiles.

Keywords: Nondestructive Testing, Active Infrared Thermography, Concrete Structures, Laboratory Testing, Weather Condition Effects, Surface Defect Assessment

Introduction

Non-destructive tests (NDT) in general and infrared thermography (IRT) are becoming the common means of inspecting civil infrastructures such as concrete and asphalt pavements especially in the field of research (Bastard et al. 2007, Szymanik et al. 2016, Lu et al. 2017). IRT is a method of NDT, which is dedicated to acquiring and processing thermal information based on the measurements made by non-contact devices (Maldague 2001). Descent accuracy, ease of use and time efficiency of IRT have made this method a favorable type of NDT that is dominantly used in pavement assessment studies (Vaghefi et al. 2011). Infrared thermal cameras record a series of live thermal images from the surface of the pavement, which allows a quick mapping of the structure by evaluating the surface temperature at each time step (Clark et l. 2003, Sakagami and Kubo 2002, Wiggenhauser 2002).

There are two types of thermography methods called passive and active IRT (Wiecek 2005). In passive IRT, the radiation that is collected from the surface of the specimen is measured without the need of applied extra heat from a heat source. In this type, the major heat source is normally the sun. In active IRT, an artificial heat source is involved in heating up the specimen for collecting the temperature gradient using a thermal camera (Ibarra-Casranedo et al. 2007, Hung et al. 2009). In this paper, active IRT is employed inside laboratory tests.

In both cases, surface temperature gradient is considered to be the major concept of an IRT approach for assessment of road pavement surface defects and delamination. As shown in Figure 4-1, the surface temperature gradient is caused by a variety of factors. One is the back and forth bouncing of the sunlight inside of the surface crack,

which heats up the walls of the crack and elevates the inner crack temperature (Sham et al. 2008). The other is the difference between the specific heat capacities of dry soil (fine sand) at the bottom of the crack and concrete, $800 \frac{J}{kg^{\circ}C}$ and $900 \frac{J}{kg^{\circ}C}$ respectively (Engineering ToolBox 2003). This shows that concrete has a higher specific heat capacity compared to dry soil, which means the temperature of the fine soil rises up faster than concrete when they are exposed to heat.

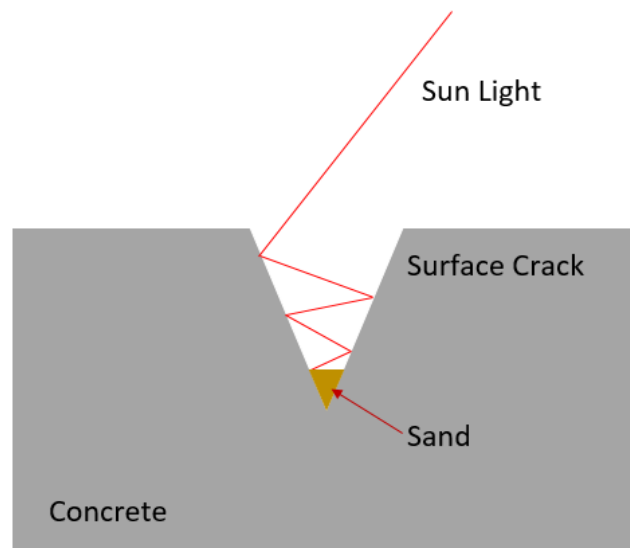


Figure 4- 1. Surface crack temperature gradient

IRT Concepts and Physics

IRT is based on processing infrared radiation, which is a form of electromagnetic radiation that is not visible to human eyes. The processed radiations that are emitted from any object with a temperature above absolute zero are then converted into electronic signals (Zissis and Wolfe 1978) and subsequently into temperature readings (Vollmer and Mollmann 2011).

The emitted electromagnetic radiation is a function of the surface temperature of the specimen. This indicates that a higher temperature will cause a greater intensity of the

emission from the surface. The wavelength of the emitted electromagnetic radiation is reversely dependent on the temperature. Therefore, for higher temperature, the wavelength is going to be shorter based on the Wien's law equation (Usamentiaga et al. 2014):

$$\lambda_{\text{peak}} = \frac{0.0029}{T} \quad (4-1)$$

The temperature gradient that is illustrated in thermography is used as the means for detection and assessment of a variety of different types of defects in pavements and civil infrastructures.

Every object that has a temperature above absolute zero, i.e. zero Kelvin, emits radiation in the infrared range, which is between 1 μm to 1000 μm in the electromagnetic spectrum (Washer et al. 2009). The following equation quantifies the energy of emitted radiation in every grey body radiator based on the Stefan-Boltzmann equation:

$$W = \epsilon \sigma T^4 \quad (4-2)$$

In which W is the energy of emitted radiation at all wavelengths, ϵ is emissivity of the surface of the specimen, σ is the Stefan-Boltzmann constant equal to $5.67 \times 10^{-8} \text{ W}/(\text{m}^2 \cdot \text{K}^4)$ and T is Temperature (K).

Temperature is the most frequently measured quantity in the industrial process by using an infrared thermal camera (Michalski et al. 2001). An infrared image is a product of the quantification of the energy that is radiated from the surface of a specimen in separate sample points of the surface that is under inspection by the thermal camera. The infrared radiation energy that is emitted from the surface of the specimen will then convert to temperature values using an infrared thermal camera.

As mentioned before, each pixel of an IR thermal image represents the temperature identity of that specific location on the surface of the specimen. However, this temperature value is not a direct result of converting emitted energy to temperature reading. The major emission entities that are received by the thermal camera are Target emissions (E_{Object}), Surrounding emissions reflected from the surface of the object ($E_{Reflected}$) and atmosphere emissions ($E_{Atmosphere}$). Therefore, the total radiation is calculated using the following equation:

$$W_{Total} = E_{Object} + E_{Reflected} + E_{Atmosphere} \quad (4-3)$$

By substituting Equation 4-2 into Equation 4-3, we can compensate for the total radiation that is received by the camera and write the following equations (FLIR A320 2008):

$$W_{Total} = \varepsilon \cdot \sigma \cdot \tau \cdot (T_{Object})^4 + (1-\varepsilon) \cdot \sigma \cdot \tau \cdot (T_{Reflected})^4 + \sigma \cdot (1-\tau) \cdot (T_{Atmosphere})^4 \quad (4-4)$$

$$T_{Object} = \sqrt[4]{\frac{W_{Total} - (1-\varepsilon) \cdot \sigma \cdot \tau \cdot (T_{Reflected})^4 - \sigma \cdot (1-\tau) \cdot (T_{Atmosphere})^4}{\varepsilon \cdot \sigma \cdot \tau}} \quad (4-5)$$

In which τ represents the transmittance of atmosphere. Figure 4-2 is a summary of all types of radiations that the camera is receiving during a heat recording process (Tran et al. 2017).

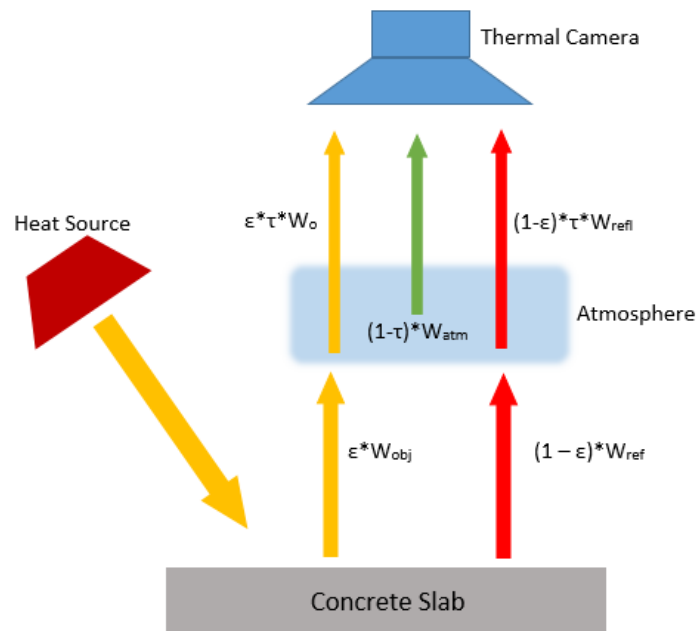


Figure 4- 2. The temperature reading process of thermal camera in experimental tests

Environmental Factors

Multiple environmental factors can affect heat transfer in concrete structures, such as wind, solar radiation effect and humidity (Manning and Holt 1983). Also other minor effects such as shades and surface roughness can alter the thermography results for inspecting surfaces and subsurface defects.

It is found that the change in ambient air temperature is the main effective parameter that can alter the thermography result and thermal camera readings. This change is the cause of temperature gradient in the concrete structure and this temperature gradient is then measured using the thermal camera. This is the main reason why the thermography is widely performed during the heating and cooling cycle of the concrete surface in the morning and later at night respectively. Since the ambient temperature is to some extent constant for a long period in the middle of the day, the concrete body and

surface is closer to temperature equilibrium with the environment surrounding it than during the heating and cooling periods of the day.

The rate of heat transfer is also affected by the wind. If the surface of the concrete slab has a higher temperature than the surrounding air, then the wind will increase the rate of convective heat transfer between the concrete and the ambient air. Therefore, the wind will decrease the temperature of the surface of the concrete and reduce the effect of radiant heating due to the cooling of the surface (Figure 4-3(A)). This phenomenon can have a reverse effect if the surface of the concrete is cooler than the ambient air, presumably in a shaded area such as the soffit of the bridge or underneath a tree. This means that the wind will expedite the heating up of the surface of the concrete by expediting the convective heat transfer from the hotter air to the cooler surface of the concrete slab (Figure 4-3(B)).

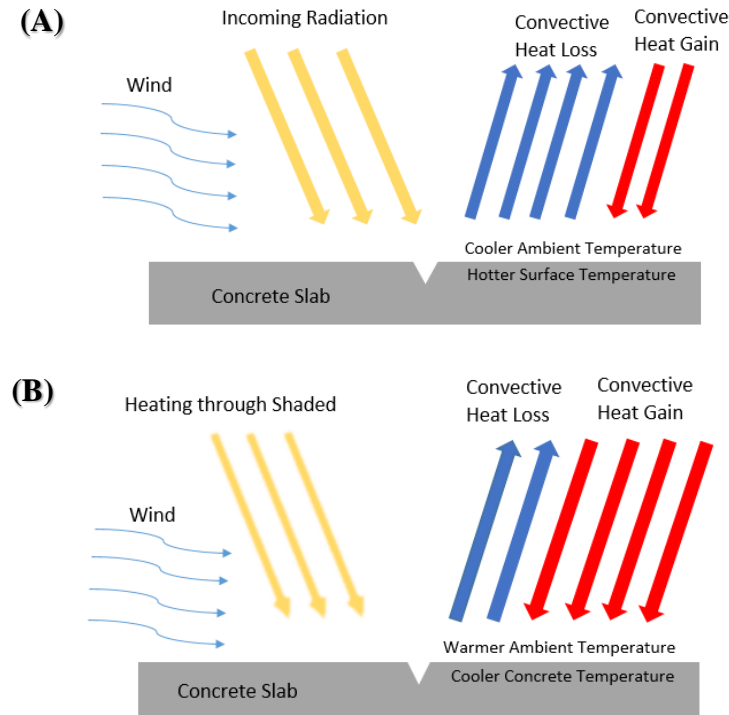


Figure 4- 3. The effect of wind on convective heat transfer on the surface of the concrete A) Under direct sun exposure B) Under indirect sun exposure (Shadow)

Relative humidity also has direct effect on convective heat transfer. Higher humidity will raise the amount for convective heat transfer coefficient and subsequently the rate of heat transfer increases (Zhang et al. 2007). Therefore, humid air will transfer more heat towards concrete than dry air. This effect along with other conditions are examined and the results are discussed in the results section of this paper.

According to the authors' previous field studies, it is found that thermography can be used to correlate the severity of the deterioration on the surface of the pavements to its measured temperature. However, the temperature readings of the thermal camera can partially be effected by weather conditions at the time of data collection (Milovanovic and Nanjad 2016). Therefore, in this paper a new testing system is introduced and an exhaustive testing procedure is conducted which will include many different types of

weather conditions which can affect the thermography. The effect of the weather conditions on thermography was observed and quantified during the cooling stage while the real time temperatures were being measured using the thermal camera.

Methodology

The temperature of most materials rises due to a variety of effects including radiation absorption. All objects with temperatures greater than absolute zero are emitters of infrared (IR) energy (Clark et al. 2003). This energy can be measured using infrared thermal cameras. However, the surrounding weather condition can have a great effect on the measurement of this energy. Current thermography related research publications and studies have asserted these effects (Milovanovic and Nanjad 2016, ASTM D4788-88 2001, Rumbayan and Washer 2014). However, not many researchers have tried to quantify them. In addition, it has not been the subject of many researches to study the limitation of the utilization of IRT imaging tools for NDT due to alterations of the results caused by different weather conditions. These phenomena are the basis of a series of tests that were conducted to study the effect of different weather conditions and crack profiles on the workability of the thermal camera and its ability to record the emitted IR energy.

A 6 by 6 by 12-inch concrete slab was casted and broke in half using a hydraulic pump. There is no reinforcement included in the slab. The strength of the concrete is measured to be around 4500 psi. This type of concrete is the main ingredient of bridge slabs and pedestrian pavements. The two pieces were then put next to each other and the space between them was filled with sand. This was to imitate the shape of crack on the surface of the specimen. This system helps us to be able to control the depth and width of

the crack with a very good precision. Figure 4-4 illustrates the measurement of width and depths and temperature of the crack on the surface of the concrete slab.

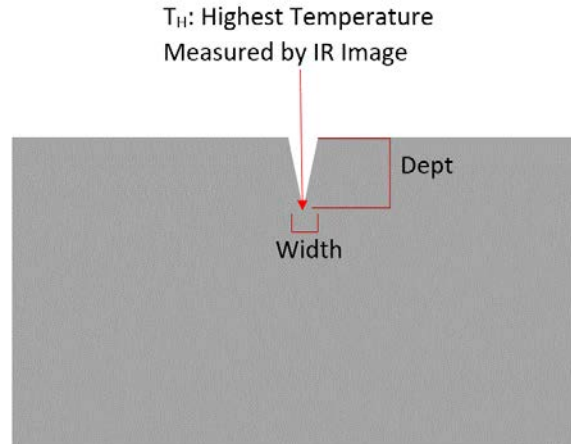


Figure 4- 4. Width, depth, and highest temperature measurements in surface cracks

The term crack ratio is used to determine the ratio between the width and depth of each crack using the following equation:

$$\text{Crack ratio} = \frac{\text{Crack depth}}{\text{Crack width}} \quad (4-6)$$

The crack ratio of 7 is used to replicate the crack profile in the field. This ratio is close to the average of the ratios of depths versus widths for nearly a hundred crack data points that have been collected from the field in the authors' previous research studies. In this study, concrete surfaces that contain cracks with a crack ratio of 7 or higher are considered as damaged surfaces. Subsequently, the depth can be calculated by knowing the crack ratio and width.

There are two main widths used in different test setups that are equal to 0.5 cm and 1 cm as shown in Figure 4-5(A). The depths are then calculated using the crack ratio and are shown in Figure 4-5(B). Other variations of the depths have also been used to

compare the results and study the effect of different crack profiles on the thermal characteristics of the crack.

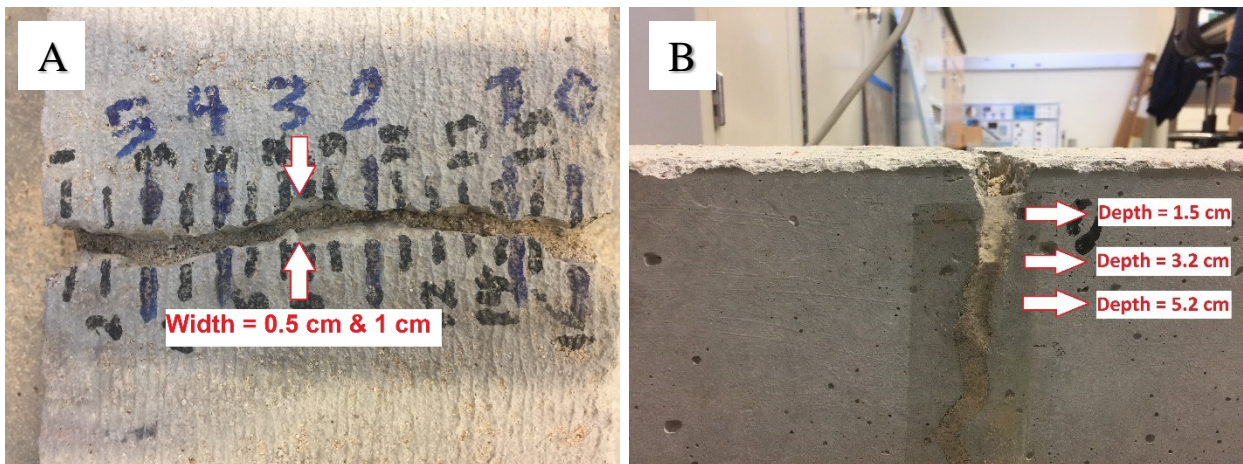


Figure 4- 5. Laboratory crack sample: A: Crack width, B: Crack depth

A 500 Watt halogen lamp is used as the heating source. Halogen lamps have the advantage of temporal stability compared to other kinds of lamps, which makes the use of this type of lamp more favorable for the active IRT tests (Maxim Integrated 2007).

The heating cycle's duration is 30 minutes for all tests. Shorter periods of heating were used but the recorded temperature data during the cooling cycle were not significant and the results were disregarded. The 30-minute heating cycle induces an excessive amount of heat on the sample. The temperature data recorded in the first 25 minutes of cooling cycle is disregarded. The remaining data until the end of the cooling cycle are considered to be more representative of what we can expect to be measured as temperature of the surface in the field.

The experimental system that is introduced in this paper is shown in Figure 4-6. This setup contains six main parts, including a 121 cm × 33 cm × 51 cm tank to control the level humidity, a concrete slab as the test specimen with an adjustable crack in the middle, a halogen lamp as the heating source, a humidity meter, ambient air temperature

reader and an infrared thermal camera. The tank is used to prevent heat from transferring to the ambient air surrounding the testing system, especially in humid heating tests.

Humidifier and fan are also added to the system, in separate tests, in order to adjust the humidity level of the system and the wind speed respectfully.

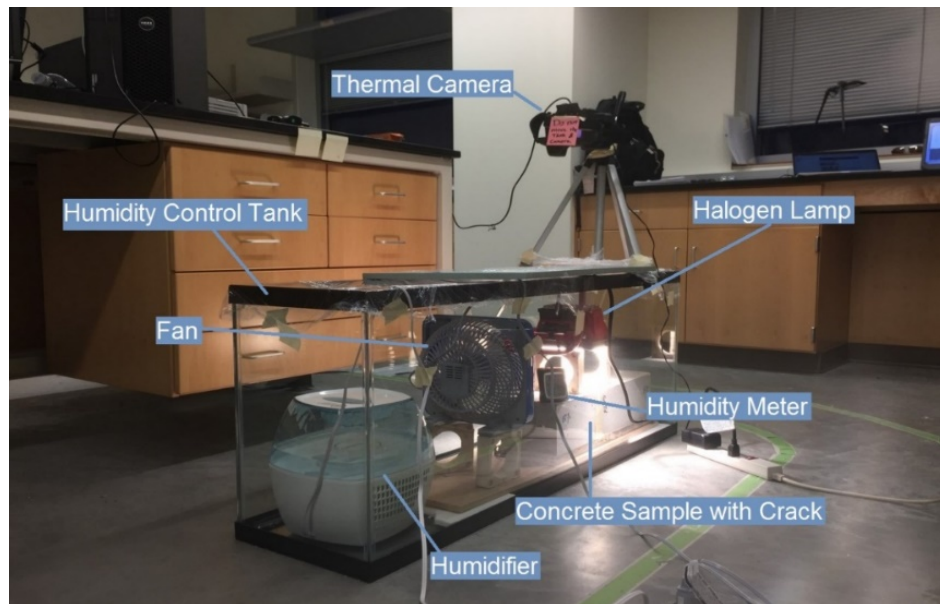


Figure 4- 6. Controlled laboratory testing system

This testing system is developed to replicate a variety of weather conditions that can affect the temperature reading of the thermal camera. The first type of lab-simulated weather condition is called “Controlled heating”. In this type, the relative humidity inside the testing system is the same as the surrounding air, at the beginning of the test. There is also no significant airflow on top of the cracked surface of the concrete slab. The second type of lab-simulated weather condition is called “Heating with airflow” (or windy condition). In this type, an airflow equal to 3.5 meters per second is introduced to the system over the cracked area of the concrete surface by using a fan. The relative humidity is also the same as the laboratory environment. The third type of lab-simulated weather condition is called “Humid heating” and includes a relative humidity equal to 80 to 85

percent before the tests starts. This amount of humidity will remain in the system very soon after the heating cycle is over. In the following the terms humidity and relative humidity will be used interchangeably.

The tank is used as both a means of controlling the humidity level and a wind tunnel for the fan. The dimensions of the tank will be used for computer modeling in future studies.

There are different types of infrared thermal cameras used to investigate anomalies in different substances. The two most common ones are uncooled micro bolometer detectors and cooled detectors, which are mostly, used in high sensitivity cameras (Rogalski 2012). A very detailed review on how these types of cameras differ in employment and structure and their historical evolution can be found in previously published literatures (Zheng and Tidrow 2009, Meola and Toscano 2012). In this test an infrared thermal camera with an uncooled micro bolometer (also known as a thermal detector) was employed. This camera is used to record the temperature gradient of the surface of the specimen and the crack. The model of the thermal camera is FLIR T430sc with a thermal sensitivity of $0.045\text{ }^{\circ}\text{C}$ at $30\text{ }^{\circ}\text{C}$ (Lu et al. 2017). The frame rate of this camera, i.e. the number of frames that is recorded in each second, is 60 Hz.

In most of the tests, the wind speed is chosen to be 3.54 m/s, with the distance of 12 inches (30.5 cm) between the fan and the cracked area on the surface of the concrete slab (Figure 4-7(A)). The humidifier is used to elevate the humidity level of the tank. The average speed of humidity addition to the air is 30% per hour when the tank is fully sealed using plastic wraps (Figure 4-7(B)).

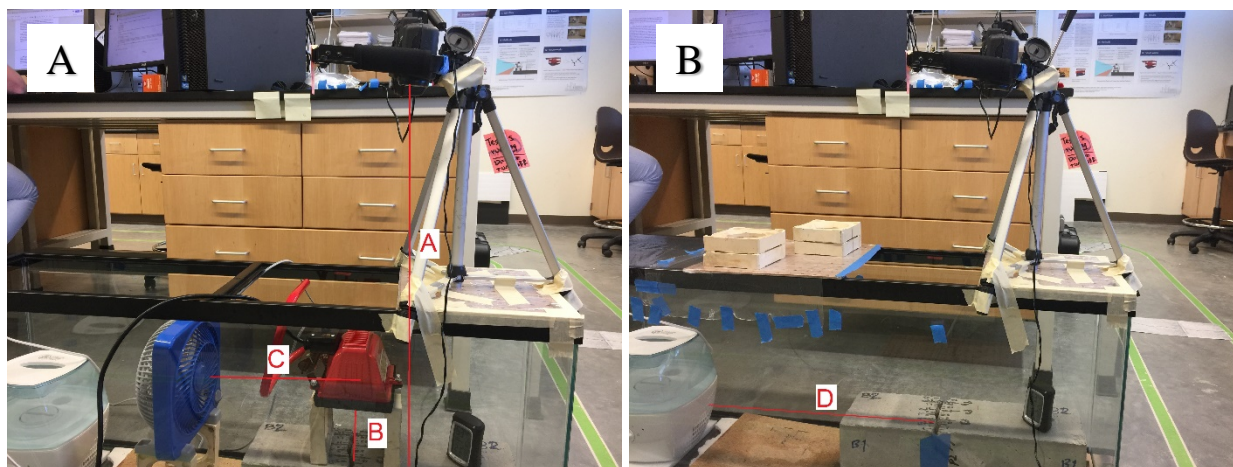


Figure 4- 7. Distance between the test facilities and crack: A: Distance between Thermal camera and crack= 70 cm, B: Distance between halogen lamp and crack= 10 cm, C: Distance between fan and crack= 30. 5 cm, D: Distance between humidifier and crack= 55 cm

There are overall 4 different sets of test setups (Table 4-1). In each set, one specific crack profile is tested under different weather conditions. A halogen lamp was used for 30 minutes to heat up the sample. In the second phase of the test, the lamp was taken away from the system and the temperature of the crack was measured for every minute for 2 hours using a thermal camera. In the case of humid heating, a humidifier was used for 1 hour before the heating process was started. During the humid heating test all parts of the tank were completely sealed using plastic wraps to maintain humidity.

Table 4- 1. Experimental tests performed inside the laboratory

Type of Test Crack Profile (cm)	Controlled Heating	Humid Heating (50 – 55%)	Humid Heating (70 – 75%)	Humid Heating (80 – 85%)	Humid Heating (~100%)	Air Flow (3.4 m/s)	Air Flow (4.23 m/s)	Air Flow (4.9 m/s)
W=0.5 – D=1.5	Case #1	--	--	Case #2	--	Case #3	--	--
W=1 – D=3.2	Case #4	--	--	Case #5	--	Case #6	--	--
W=1 – D=5.2	Case #7	--	--	Case #8	--	Case #9	Case #10	Case #11
W=0.5 –D=3.7 (2-h heating)	--	Case #12	Case #13	Case #14	--	--	--	--

To imitate foggy weather, which represents the extreme amount of humidity, almost 100%, a different setup was utilized. In this test setup, two humidifiers were used which were constantly adding humidity to the air inside the tank throughout the whole procedure. The initial humidity before starting the heating process was 99%. Although the humidity decreased after 2 hours of heating, it was increased back to 99% after 20 minutes into the cooling process. Figures 4-8(A) and 4-8(B) show the special setup for the foggy weather.

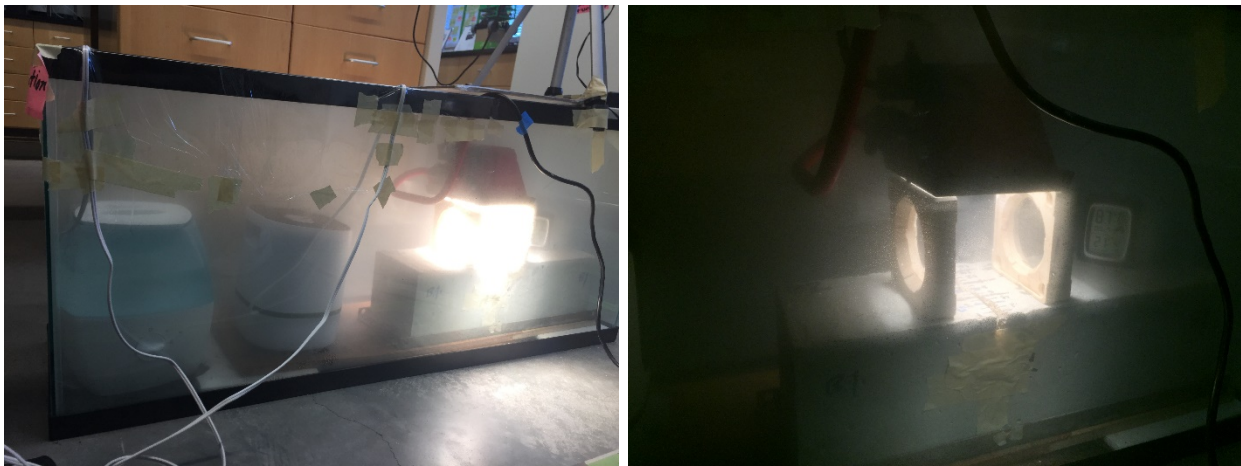


Figure 4- 8. (A & B) Foggy weather test setup (Humidity= \sim 100%)

Result

As mentioned in previous sections, infrared cameras measure the infrared radiation that is emitted from the body. The amount of the emitted infrared radiation is proportionally affected by the fourth power of absolute temperature of the surface (Equation 4-2). There is always a temperature gradient between the crack and its surrounding intact area, i.e. the area without any visible cracks. This temperature gradient is what makes IRT relevant to concrete surface inspection.

Given the fact that the temperature gradient exists throughout the cooling process, it is possible to identify the cracked areas of the surface of the concrete structures using

this method. This is an efficient tool to be able to automate the inspection process of bridges and pavements as well as concrete buildings and structures.

Figure 4-9 shows that the temperature gradient between the top and bottom side of the crack during the heating and the cooling cycles of the test in thermal images. The same pattern can be seen in these images with the top edge having a higher temperature during the heating cycle and vice versa during the cooling cycle.

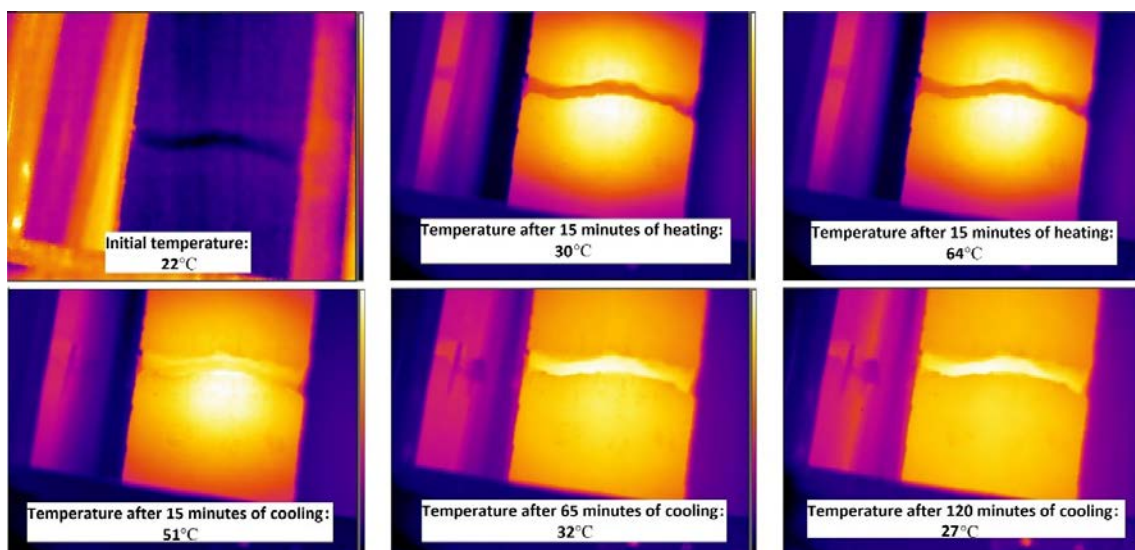


Figure 4- 9. Temperature gradient captured by the infrared thermal camera during the heating and cooling cycles (Crack sizes: Width=1cm Depth=3.2cm) - Highest surface temperature is calculated in each image

As noted before in the methodology section, the graphs will show the cooling cycle of the test process. For current testing setup, the first 25 minutes of the temperature data should be disregarded since they are not representative of what is expected to be measured when passive heating is being applied on the surface of the concrete.

Comparison of the temperature decay at the crack bottom surface versus crack top edge for controlled heating, heating with airflow (wind) and humid heating (Cases

#1 through #9)

Top edge point is chosen from an area on the sound part of the surface of the concrete that is located very close to the crack. The bottom of the crack is considered the lowest point inside of the crack, which its temperature is measurable, by the thermal camera.

Figure 4-10 shows the quantification of the temperature decay on the edge and at the bottom of the crack under three different weather conditions. The rate of temperature decay helps to quantify significance of the effect of a type of weather condition on the temperature reading of the camera throughout the testing process. This crack is 1 cm wide and 5.2 cm deep. As shown in these graphs, the temperature gradient exists throughout the cooling process of the concrete slab in three different tests conducted in laboratory experiments. Temperature of the top edge of the crack is higher compared to the temperature at the bottom of the crack. The reason for this phenomenon is that the top surface of the crack, which is located on the concrete section, is closer to the heating source, than the bottom of the crack, which is mostly dry fine sand. However, during the cooling process, the surface dissipates more heat than the bottom of the crack because it is more exposed to air than the bottom side. Figure 4-10(A), is the temperature decay pattern in controlled heating. Figure 4-10(B) and Figure 4-10(C) represent the same pattern for heating with airflow and humid heating respectively. In all cases, the top edge of the crack dissipates heat faster than the bottom side.

This difference in temperatures, however, will reduce relatively quickly during the heating cycle. As can be seen in Figure 4-10(A) the temperature of the edge surface is 44°C while the temperature of the bottom of the crack is 45.5°C. The 1.5°C temperature

gradient stays the same for most of the cooling cycle until it gradually reduces to 1°C at the end of the two-hour reading.

The same tests have been carried out on cracks with varying profiles and under different weather conditions (Figures 4-10(B) and 4-10(C)). The same trend was observed for cracks with varying crack ratios. However, the temperature gradient is more severe in heating with airflow inside the system and is about 3°C at a point in the middle of cooling cycle. Eventually, the temperature gradient resumes to 1°C for all three types of weather conditions at the end of cooling cycle.

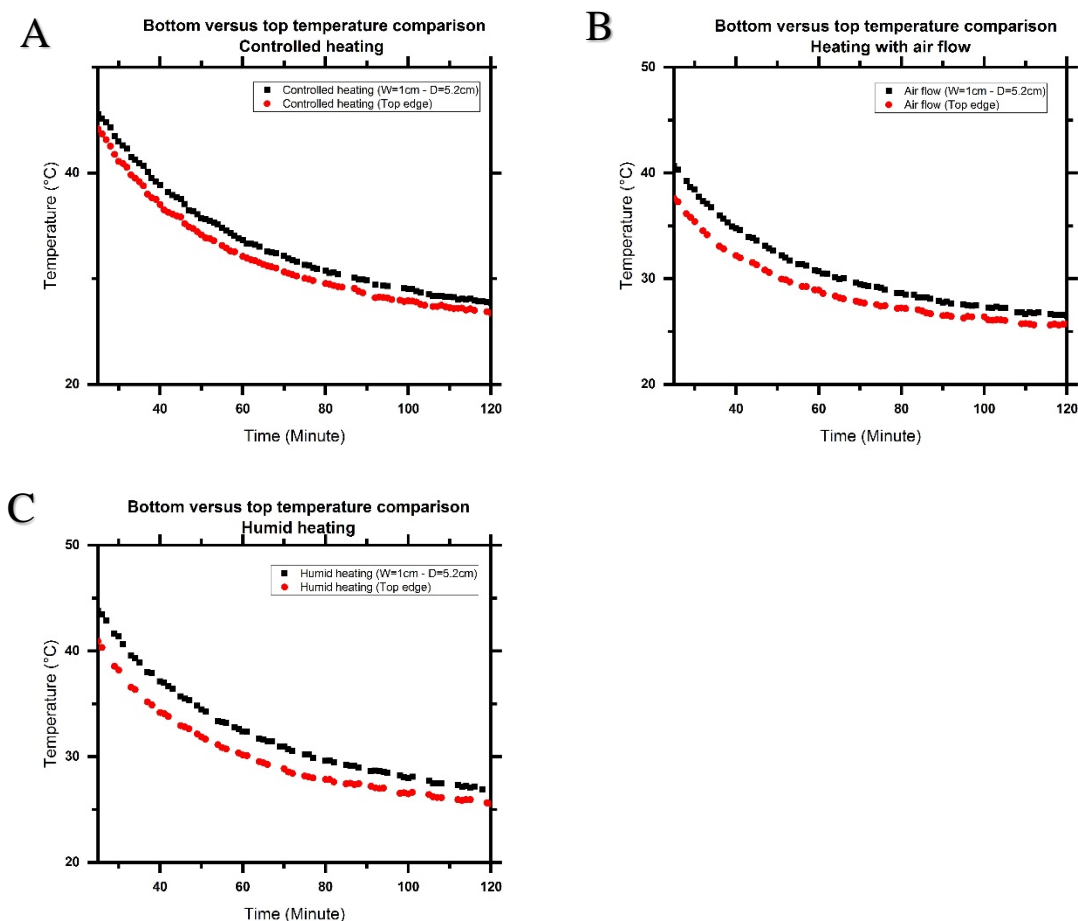


Figure 4- 10. Temperature decay versus time for top edge and bottom of crack in 3 different test sets, A) Controlled heating, B) heating with airflow and C) moist heating

Comparison of the Effect of Different Humidity Levels on Temperature Decay of the Crack in Humid Heating (Cases #10, #11, #12, #13 And #14)

It is found that the ambient air temperature dissipates faster when the humidity is higher in the air. For instance, when the humidity is 70 percent (Figure 4-11(B)), temperature decay has a steeper slope compared to humidity of 55 percent in the second test (Figure 4-11(A)). Therefore, the temperature after 1 hour of cooling is around 1°C higher for the test that has a lower humidity in the air.

It should be noted that for this set of tests, the heating cycle duration is 2 hours.

That is to have a higher temperature gradient and a better visualization of the temperature comparison.

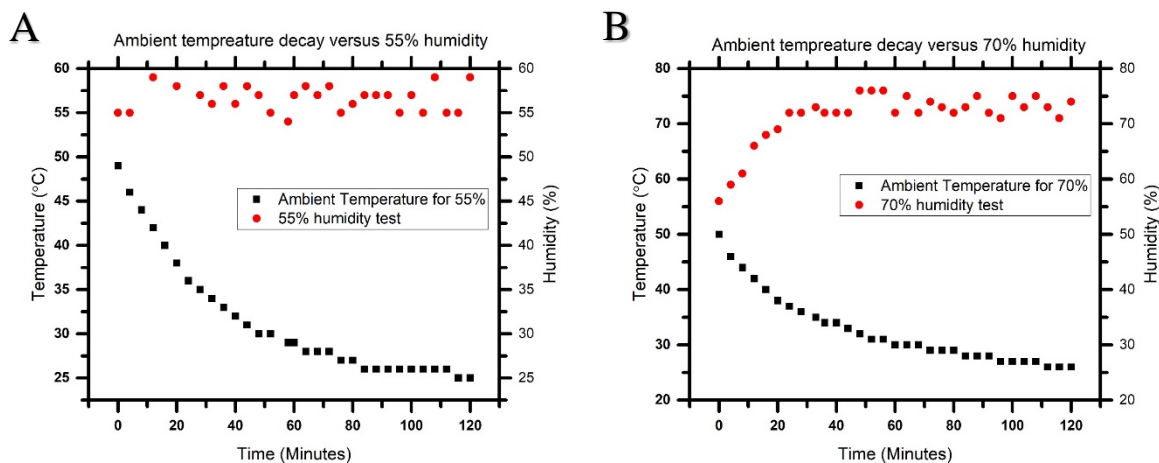


Figure 4- 11. Relation between humidity and ambient air temperature decay: A: For 55% humidity, B: For 70% humidity

Figure 4-12 shows the rate of humidity change inside the system for different humidity tests.

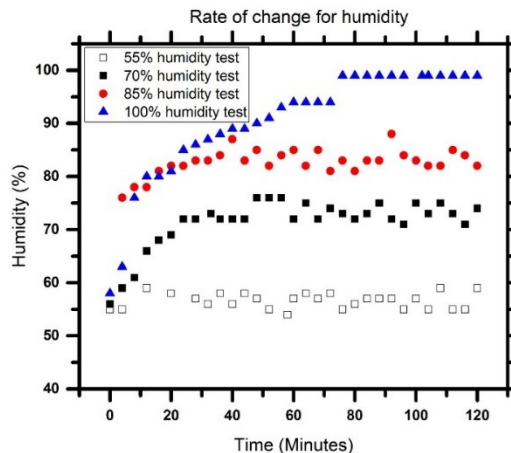


Figure 4- 12. The change in humidity levels versus time

Prior the start of the heating process, humidity was raised up to 80%. However, as shown in Figure 4-13, the humidity decreases during the two hours of the heating process. In this graph, the rate of change for humidity during the cooling process is plotted for four different tests with different amount of humidity percentages. The humidity level never went below the target amount and it did not increase more than 5 percent above it. This helped to keep the humidity consistent throughout the testing period. However, the humidity in the foggy weather test reaches the highest amount, which is plus 99%, after 75 minutes into the cooling process.

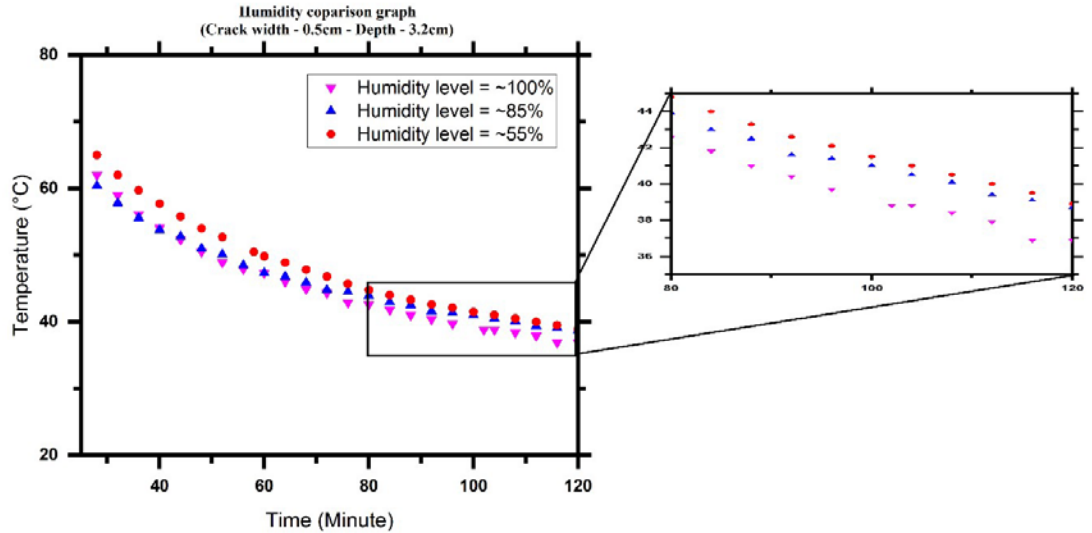


Figure 4- 13. Time versus temperature decay graph for different humidity levels

As shown in Figure 4-13, when humidity is introduced into the system and regardless of the level of this humidity, the temperature of the crack is going to dissipate with a higher rate compared to the system with regular humidity content, i.e. 20%. Therefore, throughout the cooling process of the test, the temperature at the bottom of the crack in humid air is always lower to controlled test with regular humidity.

The same concept holds when the air has extremely high humidity equal to 99% that occurs in foggy weather conditions, but the rate is completely different. In the 99% humidity test, the temperature is lower throughout the cooling process compared to 55%, 70% and 85% humidity. 100 minutes into the cooling cycle, temperatures of the crack are 41°C for 55% humidity, 40.5 °C for 85% humidity, 38.8 °C for 99% humidity and finally 36.4 °C for 20% humidity. This clearly shows that by adding humidity into the system the temperature rises for at least 2 °C up to around 5 °C depending on the level of humidity. However, at the same time, it can also be observed that by adding more humidity to the ambient air, this shift in crack temperature reduces to a lower amount.

The comparison of the effect of different weather conditions and various crack depths on temperature decay of the crack and the temperature readings of thermal camera (Cases #1 through #9)

Humidity and wind are the two major ambient air conditions, which have huge effects on the temperature of the crack and functionality of the camera. Figure 4-14 shows temperature readings during the cooling cycle under each weather condition.

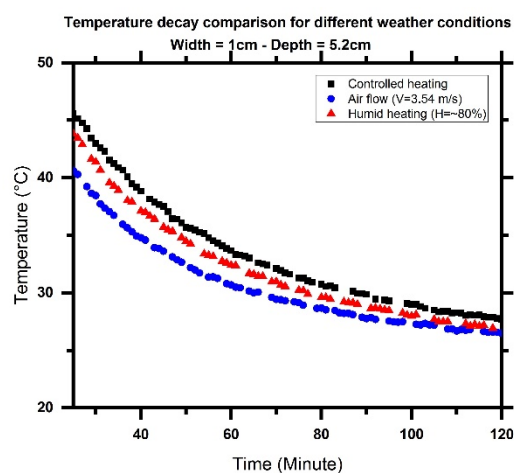


Figure 4- 14. The effect of different weather conditions on temperature reading of the thermal camera for a crack with 1 cm width and 5.2 cm depth

As mentioned in the methodology section, in the current testing method, humidity in the air is replicated using a humidifier. The humidity was maintained between 80 to 85 percent for the humid test. In addition, to replicate the wind, a fan was used. The wind velocity on top of the crack was measured to be 3.54 m/s for this test. As expected, the temperature of the crack decays faster when there is airflow present inside the system. The reason is that the wind contributes to the convection process on top of the crack by expediting the movement of the local air around the surface of the concrete. Additionally, the humid air will preserve the heat inside the crack. Therefore, the decay of the

temperature level inside the crack is going to be faster when humidity was introduced into the system (Figure 4-15).

As mentioned earlier, this phenomenon happens due to the higher heat capacity of water compared to dry air. Therefore, in humid systems, which has a humidity around 80%, the temperature of the crack is lower than the normal system, which has a humidity level equal to 20%.

In order to calculate the magnitude of the effect of each weather condition on the temperature readings of the camera, the percentage of difference (POD) between each test condition is measured using the following formula:

$$\frac{|T1 - T2|}{\frac{(T1 + T2)}{2}} \times 100 \quad (4-7)$$

In which, T1 is the temperature in one test setup and T2 is the temperature in another test setup.

Humidity has the lowest effect on the temperature of the crack throughout the cooling process with an average percentage of the difference equal to 5.8 percent when it is compared to controlled heating test results. On the other hand, the average PODs for windy weather compared to controlled heating is 11.3 percent. This indicates that wind has a much higher effect, around 2 times, on the temperature of the crack than the humidity.

The same sets of tests have been conducted on cracks with the same width but varying depth (Figure 4-15(A) and 4-15(B)). This was done to study the potential change in the amount of effect that each weather condition will have on shallower cracks.

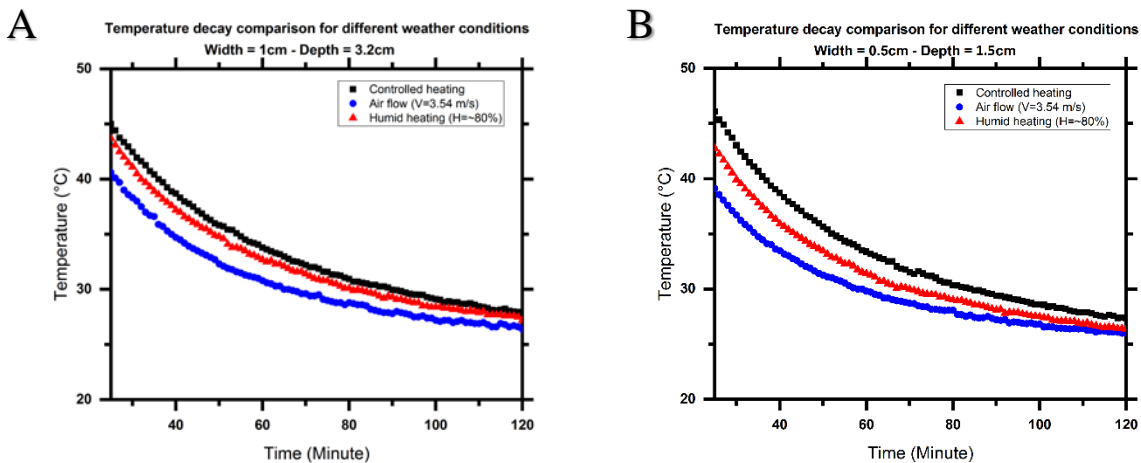


Figure 4- 15. Comparison of the effect of different weather conditions on temperature reading of the thermal camera for cracks with varying crack profiles: A: For width=1 cm and depth=3.2 cm, B: For width=0.5 cm and depth=1.5 cm

The change between different crack depths is quantified using the POD concept (Figure 4-16). As is shown in this bar graph, the increase in depth causes a decrease in the average of the PODs. Therefore, the temperature reading of the camera for deeper cracks is more prone to changes due to the weather condition compared to shallower cracks.

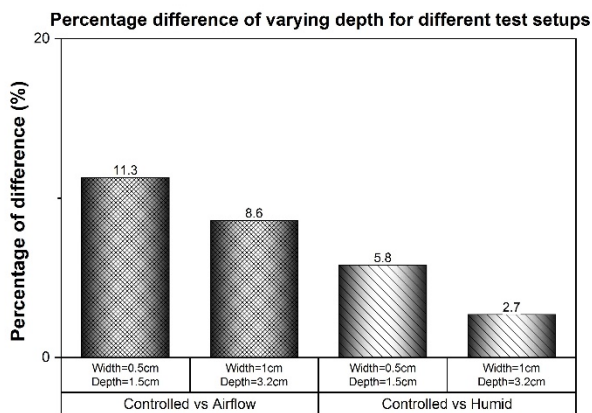


Figure 4- 16. Comparison of the percentage of difference for varying depths when exposed to different weather conditions

Comparison of the effect of different air velocities on temperature decay of the crack (Cases #15, #16 and #17)

Three different wind velocities were introduced into the system in the following test setup. The velocity in each section of this test was measured on top of the cracked area of the concrete sample. The measured velocities are equal to 5.01, 4.23 and 3.54 meters per second. In this test, the possible effect of wind velocity on temperature reading of the thermal camera is measured.

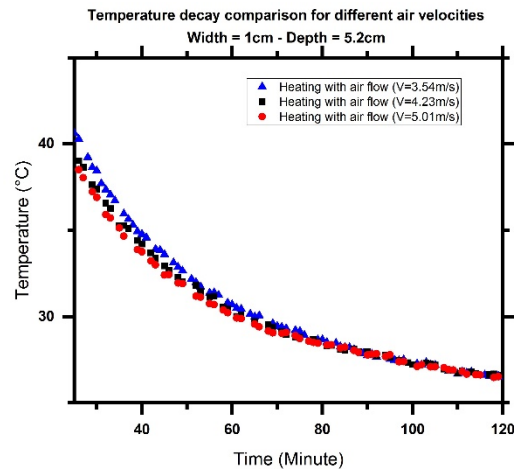


Figure 4-17. Temperature decay in different wind (air) speeds

As can be seen in Figure 4-17, the temperature gradient between different wind velocities is close, especially at the end of cooling cycle. The average percentage difference throughout the cooling process between the highest and lowest velocities is less than 5%. This number reaches to as low as 2% near the end of the cooling process. This indicates that at the end of the cooling process, the temperature of the crack is anticipated to be close to an average amount of 26.5 degrees Celsius, regardless of the wind velocity that is introduced into the system in each test.

Conclusion

The effects of ambient air conditions on the reading of infrared thermal cameras have been one of the major concerns of the researchers in the thermography field. Although these effects have been mentioned in previous research attempts, the significance of the effect of ambient air conditions on the detection of defects in concrete structures has not been quantified and studied in detail.

This paper covers a systemic study, including the physics and concepts related to active IRT for concrete and the effect of the ambient air condition on surface defect assessment. A weather controlled testing system is developed inside the laboratory in order to imitate different weather conditions that can happen in the field and surrounding concrete structures. More than 17000 test data points in over 35 different test setups have been collected in a time span of two months. All the tests have been performed inside a laboratory and a halogen lamp was used as the heating source. The goal for this study was to address the direct and indirect effects of ambient air and weather conditions, including humidity, wind, and ambient air temperature on the performance and reliability of the IRT for surface crack assessment. The large amount of test results that are collected in this study are being used to improve the accuracy of the use of IRT for assessing the surface defects in concrete structures. In addition, the effect of different crack profiles on the performance of IRT was also studied.

According to the finding of this research, wind has a bigger influence than humidity level on the temperature of the crack and the readings of the camera. According to the test results, when the air flows on top of the surface crack with a speed of 3.2 m/s, the temperature of the crack drops up to 3.5°C compared to the temperature of the crack

in controlled heating. This is while in humid heating, where humidity level equals 80%, the temperature rises with the amount of around 1.7 °C. In other words, the temperature shift in cracks that are exposed to a windy weather is almost 2 times more intense than in humid weather. Although both wind and humidity can affect the temperature of the crack, the different wind speeds and humidity levels have roughly the same amount of effect on the temperature.

References

- ASTM D4788-88 2001. *Standard Test Method for Detecting Delaminations in Bridge Decks Using Infrared Thermography*. ASTM International: West Conshohocken, PA, USA.
- Bastard C.L., Baltazart V., Wang Y., Saillard J. 2007. *Thin-pavemet thickness estimation using GPR with high-resolution and superresolution methods*. IEEE TRANSACTIONS ON GEOSCIENCE AND REMOTE SENSING, 2511-2519.
- Clark M.R., McCann, D.M., Forde M.C.* 2003. Application of infrared thermography to the non-destructive testing of concrete and masonry bridges. NDT&E International, Vol. 36 No. 4, 265-275.
- Engineering ToolBox 2003. *Heat Capacity*. [online] Available at: https://www.engineeringtoolbox.com/heat-capacity-d_338.html.
- FLIR A320 2008. *FLIR A325 User's Manual*. FLIR Systems: Boston, MA, USA.
- Hung Y., Chen Y., Ng S., Liu L., Huang Y., Luk B., Ip R., Wu C., Chung P. 2009. *Review and comparison of shearography and active thermography for nondestructive evaluation*. Mater. Sci. Eng. R Rep. 64, 73–112.
- Ibarra-Casranedo C., Genest M., Piau J.M., Guibert S., Bendada A., Maldague X.P., Chen C. 2007. *Ultrasonic and Advanced Methods for Nondestructive Testing and Material Characterization*. Active Infrared Thermography Techniques for the Non-Destructive Testing of Materials, Chen, C.H., Ed.; World Scientific: Singapore, Singapore, 325–348.

- Lu Y., Golrokh A.J., Islam M.A 2017. Concrete pavement service condition assessment using infrared thermography. Hindawi publications, 1-8.
- Maldague X. 2001. Theory and Practice of Infrared Technology for Nondestructive Testing. Wiley: New York, NY, USA.
- Manning D.G., Holt F.B. 1983. *Detecting Deterioration in Asphalt-Covered Bridge Decks*. Transportation Research Record, 10-20.
- Maxim Integrated 2007. *Replace Inefficient MR16 Halogen Lamps with LEDs*. <https://www.maximintegrated.com/en/app-notes/index.mvp/id/4086>, Reference schematic 4086, September 25.
- Meola C. & Toscano C. 2012. Non-Destructive evaluation of carbon fiber reinforced polymers with ultrasonics and infrared thermography: An overview on historical steps and patents. Recent Patents Mater. Sci., 5, 48–67.
- Michalski L., Eckersdorf K., Kucharski J., McGhee J. 2001. *Temperature Measurement Second Edition*. John Wiley & Sons Ltd, West Sussex UK.
- Milovanovic B. & Nanjad Pecur I. 2016. *Review of Active IR Thermography for Detection and Characterization of Defects in Reinforced Concrete*. Journal of Imaging, 1-27.
- Rogalski A. 2012. *Progress in focal plane array technologies*. Progr. Quantum Electron, 36, 342–473.
- Rumbayan R. & Washer G. A. 2014. *Modeling of Environmental Effects on Thermal Detection of Subsurface Damage in Concrete*. Research in Nondestructive Evaluation, Tylor and Francis Group, 235-252.
- Sakagami T. and Kubo S. 2002 Development of a new non-destructive testing technique for quantitative evaluations of delamination defects in concrete structures based on phase delay measurement using lock-in thermography. Infrared Physics & Technology, Vol. 43 No. 3, 311-316.
- Sham F C., Chen N., Long L. 2008. *Surface crack detection by flash thermography on concrete surface*. The British Institute of Non-Destructive Testing.

- Szymanik B., Frankowski P.K., Chady T., Robinson C., Chelliah A.J. 2016. Detection and inspection of steel bars in reinforced concrete structures using active infrared thermography with microwave excitation and eddy current sensors. MDPI, 1-16.
- Tran Q.H, Han D., Kang Ch., Haldar A., Huh J. 2017. Effects of Ambient Temperature and Relative Humidity on Subsurface Defect Detection in Concrete Structures by Active Thermal Imaging. Sensors, 1-18.
- Usamentiaga R., Venegas P., Guerediaga J., Vega L., Molleda J., Bulnes F.G. 2014. *Infrared Thermography for Temperature Measurement and Non-Destructive Testing*. Sensors, ISSN 1424-8220, 12305-12348.
- Vaghefi Kh., Silva H., Harris D., Ahlborn Th. 2011. Application of thermal IR Imagery for concrete bridge inspection.
- Vollmer M., Mollmann K.P. 2011. *Infrared Thermal Imaging: Fundamentals, Research and Applications*. Wiley, Weinheim, Germany.
- Washer G. A., Fenwick R. G., Bolleni N. K. 2009. *Development of Hand-held Thermographic Inspection Technologies*. University of Missouri Columbia and Missouri Department of Transportation.
- Wiecek B. 2005. *Review on thermal image processing for passive and active thermography*. In Proceedings of the 27th Annual International Conference of the IEEE Engineering in Medicine and Biology, Shanghai, China, 686–689.
- Wiggenhauser H. 2002. *Active IR-applications in civil engineering*. Infrared Physics & Technology, Vol. 43 No. 3, 233-238.
- Zhang J., Gupta A., Baker J. 2007. Effect of Relative Humidity on the Prediction of Natural Convection Heat Transfer Coefficients. Heat Transfer Engineering, 28(4), 335-342.
- Zheng L. & Tidrow M. 2009. Analyses of infrared focal plane array figure of merit and its impact on sensor system trades. Infrared Phys. Technol., 52, 408–411.
- Zissis G.I. & Wolfe W.L. 1978. *The Infrared Handbook*. Technical report, DTIC document.

CHAPTER FIVE: CONCLUSION

Developing an efficient approach to assess the distresses such as cracks and air voids on top or near the surface of concrete and asphalt roadways is a great challenge for engineers. Infrared thermal imaging inspection, a branch of non-destructive testing (NDT), is a promising method that can help us towards achieving this goal. Infrared thermography (IRT) can be used for the inspection of surface and subsurface defects on or inside concrete and asphalt pavements. What is puzzling though is the fact that the raw thermal images by themselves cannot be a reliable substitute for this testing technique. Therefore, processed thermal images can help us to better understand and investigate the acquired data from thermal cameras.

IRT is relatively easy to employ and it is a reliable NDT technique. By using IR cameras, we can capture temperature gradients on the surface of asphalt and concrete pavements at certain time windows during both heating and cooling cycles. IRT's one-side deployment makes it favorable for bridge and pavement assessment since in these types of structures only one side of the structure is accessible. On the other hand, there is a limited access to uniform heating in active IRT. This shortcoming makes it hard to employ image processing on thermal images that are lacking clear contrast. Subsurface defects, like delamination, are detectable only if they are close to the surface of concrete and asphalt pavements. The method works best when there is a thermal contrast present on the surface of the target.

For subsurface inspection, we were able to study the ability of thermography to locate defects underneath the surface of concrete specimens. Studying the effect of delamination depth on the temperature gradient will assist the better understanding of the effectiveness of thermography in monitoring applications. By using processed thermal images, we were able to detect the presence of air voids underneath concrete structures. We investigated the effect of the depth of these subsurface defects based on the processed images. It was found that the depth in which the defect is located has a major effect on how well it can be recognized by the thermal camera. The best results were acquired from defects that were imbedded close to the surface, up to 5 mm with an accuracy of more than 70%. A computer simulation of the test showed the same trend as seen inside the laboratory.

For surface inspection, a relation between crack temperature and its profile is studied. Based on the point-wise normalized temperatures, the areas inside the cracks always have higher temperatures than their surrounding areas. In this work, we proposed a crack detection approach for inspecting pavements in a more efficient and accurate manner. A new approach based on normalization of the temperatures shows that deeper cracks have higher temperature in the temperature profile that is captured by using a thermal camera. Correlation between temperature and depth of crack was higher ($R^2=70\%$) compared to the temperature and width of crack ($R^2=50\%$). The temperature data represented in the graphs are normalized based on the localized average surface temperatures.

To address and assess the side effects of weather conditions on thermography, a full experimental study of different weather conditions have been done inside the

laboratory. Temperature reading during the cooling cycle shows the effect of relative humidity (= 80%) and wind (=3.5 m/s or 7.8 mph) on the temperature reading of the camera. Heating under normal conditions (humidity = 16% and no wind) is taken as control. It is found that cracks heat up less and lose heat faster in humid conditions. It is also found that the effect of wind is significantly greater than humidity on the readings of the surface temperature gradient for different crack profiles (with POD of 11.3% versus 5.8%, respectively). In addition, it is found that deep cracks are more prone to the effects of humidity than shallow cracks.

Studying different aspects of IRT may help in development of a system to automate the inspection of surface and subsurface defects in pavements by using thermal imagery. Studying the effects of weather condition on the readings of the thermal camera can also assist us to be able to use the technology for field inspection in a wider time window.